Journal Pre-proofs

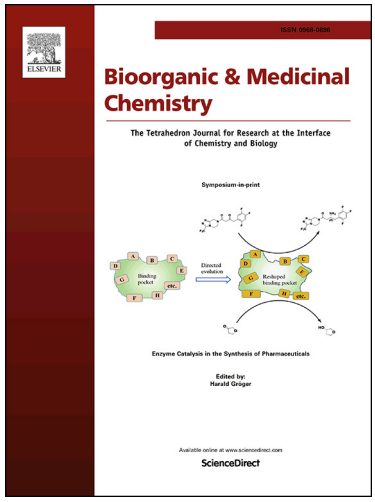

Piperidine and piperazine inhibitors of fatty acid amide hydrolase targeting excitotoxic pathology

Manjunath Lamani, Michael S. Malamas, Shrouq I. Farah, Vidyanand G. Shukla, Michael F. Almeida, Catherine M. Weerts, Joseph Anderson, JodiAnne T. Wood, Karen L.G. Farizatto, Ben A. Bahr, Alexandros Makriyannis

PII: S0968-0896(19)31023-5
DOI: https://doi.org/10.1016/j.bmc.2019.115096
Reference: BMC 115096

To appear in: *Bioorganic & Medicinal Chemistry*

Received Date: 19 June 2019
Revised Date: 7 September 2019
Accepted Date: 8 September 2019

Please cite this article as: Lamani, M., Malamas, M.S., Farah, S.I., Shukla, V.G., Almeida, M.F., Weerts, C.M., Anderson, J., Wood, J.T., Farizatto, K.L.G., Bahr, B.A., Makriyannis, A., Piperidine and piperazine inhibitors of fatty acid amide hydrolase targeting excitotoxic pathology, *Bioorganic & Medicinal Chemistry* (2019), doi: https://doi.org/10.1016/j.bmc.2019.115096

Piperidine and piperazine inhibitors of fatty acid amide hydrolase targeting excitotoxic pathology

Manjunath Lamani [1], Michael S. Malamas [*1], Shrouq I. Farah [1], Vidyanand G. Shukla [1], Michael F. Almeida [2], Catherine M. Weerts [1], Joseph Anderson [1], JodiAnne T. Wood [1], Karen L.G. Farizatto [2], Ben A. Bahr [2] and Alexandros Makriyannis [1].

[1]Center for Drug Discovery and Departments of Chemistry and Chemical Biology and Pharmaceutical Sciences, Northeastern University, Boston, MA 02115, USA; [2]Biotechnology Research and Training Center, University of North Carolina Pembroke, Pembroke, NC 28372, USA.

Abstract

FAAH inhibitors offer safety advantages by augmenting the anandamide levels "on demand" to promote neuroprotective mechanisms without the adverse psychotropic effects usually seen with direct and chronic activation of the CB1 receptor. FAAH is an enzyme implicated in the hydrolysis of the endocannabinoid *N*-arachidonoylethanolamine (AEA), which is a partial agonist of the CB1 receptor. Herein, we report the discovery of a new series of highly potent and selective carbamate FAAH inhibitors and the evaluation for neuroprotection. The new inhibitors showed potent nanomolar inhibitory activity against human recombinant and purified rat FAAH, were selective (>1000-fold) against serine hydrolases MGL and ABHD6 and lacked any affinity for the cannabinoid receptors CB1 and CB2. Evaluation of FAAH inhibitors **9** and **31** using the *in vitro* competitive activity-based protein profiling (ABPP) assay confirmed that both inhibitors were highly selective for FAAH in the brain, since none of the other FP-reactive serine hydrolases

in this tissue were inhibited by these agents. Our design strategy followed a traditional SAR approach and was supported by molecular modeling studies based on known FAAH cocrystal structures. To rationally design new molecules that are irreversibly bound to FAAH, we have constructed "precovalent" FAAH-ligand complexes to identify good binding geometries of the ligands within the binding pocket of FAAH and then calculated covalent docking poses to select compounds for synthesis. FAAH inhibitors **9** and **31** were evaluated for neuroprotection in rat hippocampal slice cultures. In the brain tissue, both inhibitors displayed protection against synaptic deterioration produced by kainic acid-induced excitotoxicity. Thus, the resultant compounds produced through rational design are providing early leads for developing therapeutics against seizure-related damage associated with a variety of disorders.

Keywords: Fatty acid amide hydrolase (FAAH); FAAH inhibitor; monoacylglycerol lipase (MGL); N-arachidonoylethanolamine; cannabinoid CB1 receptor; endocannabinoid system; hippocampus; neuroprotection.

1. Introduction

Fatty acid amide hydrolase (FAAH)[1] is an integral membrane-bound enzyme that primarily degrades the N-acylethanolamines (NAEs) family of signaling biolipids, including N-arachidonoylethanolamine (anandamide, AEA), palmitoylethanolamine (PEA), and oleoylethanolamine (OEA). AEA was identified as an endogenous partial agonist of the cannabinoid receptors CB1 and CB2[2], two members of the endocannabinoid system (eCB). The eCB consists of the known G-protein-coupled cannabinoid receptors CB1 and CB2,[3, 4] the endogenous lipid ligands arachidonoylethanolamine (anandamide, AEA)[2] and 2-

arachidonoylglycerol (2-AG),[5] as well as their primary hydrolytic enzymes FAAH and monoacylglycerol lipase (MGL)[6]. The CB1 receptors are widely distributed throughout the brain and mediate the majority of the cannabinoid effects in the central nervous system (CNS).[7] In contrast, the CB2 receptors are primarily found in cells of immune origin,[8] including microglia, although low-level expression has been reported in healthy neurons.[9] There is an abundance of evidence to support that dysfunction of the eCB system leads to a wide range of neuropathological disorders, such as obesity, immunological dysfunction, metabolic syndromes, psychiatric conditions, epilepsy, and neurodegenerative diseases, including Parkinson's disease and Alzheimer's disease[10-13].

Activation of CB1 receptors can protect against hyperexcitability induced neuronal damage.[14-18] Hence, FAAH inhibition and increased AEA levels offer the opportunity to protect neurons against excitotoxic damage. Moreover, activation of the CB1 receptors with exogenous natural and synthetic cannabinoids found to exert neuroprotective functions in several models of neurotoxicity[19, 20] and disruption of CB1 receptors signaling caused an increase in excitotoxic vulnerability and seizure susceptibility, as well as attenuation of neuronal maintenance.[17, 21, 22] Notably, studies have shown that neuronal depolarization triggered by excitotoxic kainic acid (KA) in animals resulted in marked increase of anandamide levels leading to neuroprotection,[23-25] while the tissue concentrations of 2-AG remained unchanged. In this paper, we discover new FAAH inhibitors and study their role in neuroprotection and epilepsy.

We hypothesize that the use of FAAH inhibitors will lead to "on demand" augmentation of anandamide as a response to sustained neuronal depolarization, as seen to occur with seizure activity, and contribute to the activation of CB1 receptors and trigger protective mechanisms against a neurotoxic insult.[26-28] Recent findings have reinforced the role of FAAH inhibitors in

neuroprotection by reducing hippocampal excitability[29] and seizure severity.[14] Furthermore, FAAH inhibitors offer safety advantages over CB1 agonists in neuroprotection by increasing the levels of AEA "on-demand" to activate CB1 receptors, while lacking the adverse psychotropic effects usually seen with direct and persistent stimulation of CB1 receptors[30].

Herein, we report a new series of highly selective FAAH inhibitors and their assessment to protect against KA-induced excitotoxic damage as a potential treatment for epileptic seizures as well as other disorders involving excitotoxicity in vulnerable brain regions like the hippocampus. The FAAH inhibitors were evaluated for neuroprotection against (1) molecular indicators of pathology in the excitotoxic hippocampal slice model, and (2) pathogenic indicators after intrahippocampal injection of excitotoxin. Our results indicate that after excitotoxic insults, FAAH inhibition with **9** and **31** protects against neural compromise in hippocampal slices and reduces seizure activity and seizure-associated damage in rats. These findings provide further evidence for the therapeutic potential of FAAH inhibition against excitotoxic brain injury.

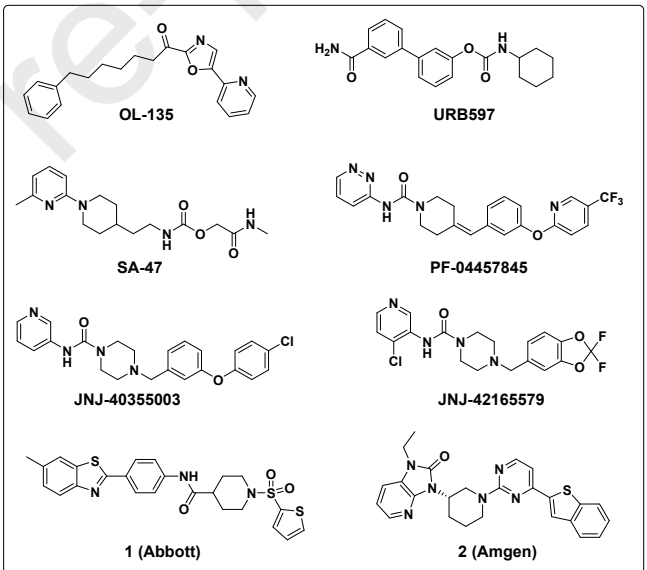

Figure 1. Known FAAH inhibitors

1.1 Known FAAH Inhibitors

Many FAAH inhibitors have been reported[31, 32] during the last decade, mostly represented by three distinct structural classes. These inhibitors are grouped as follow: (1) *covalent reversible inhibitors*, such as α-ketoheterocycle OL-135[33]; (2) *covalent irreversible inhibitors* exemplified by aryl-carbamates (e.g. URB597[34], SA-47[35]) and aryl-ureas (e.g. PF-04457845[36], JNJ-40355003, JNJ-42165579) and (3*) non-covalent reversible inhibitors* exemplified by benzothiazole 1

(Abbott)[37] and benzothiophene 2 (Amgen)[38]. To date, only a few FAAH inhibitors have entered clinical trials for evaluation in various diseases. Pfizer's PF-04457845 a highly potent and selective inhibitor with a robust druggability profile was evaluated in Phase II clinical trials (NCT00981357) as an analgesic in patients with osteoarthritis pain but was found to be ineffective[39]. Also, PF-04457845 is currently under investigation for central-related pathologies for treating post-traumatic stress disorders (PTSD; NCT02216097), cannabis related withdrawal symptoms (NCT03386487), cannabinoid receptor augmentation on the facilitation of fear conditioning (NCT01665573) and Tourette's syndrome (NCT02134080). Furthermore, other companies as well are studying FAAH inhibitors in clinical trials including Vernalis V158866 for neuropathic pain following spinal cord injury (NCT01748695) and Sanofi-Aventis SSR411298 as a treatment for major depressive disorder in elderly patients (NCT00822744).

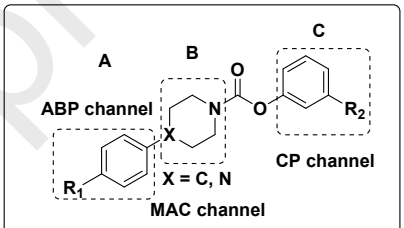

Figure 2. Expolre regional hydrophilic paterns of ligand substitution to improve druggability

In an effort to synthesize selective and potent inhibitors of FAAH for neuroprotection, we have examined series of carbamates derived from piperidine and piperazines motifs (Fig. 2).

2. Chemistry

2.1 Structural features of FAAH in inhibitor design

FAAH is a membrane bound serine hydrolase enzyme defined with a highly conserved primary sequence rich in serine and glycine residues and characterized by a unique Ser241-Ser217-Lys142 catalytic triad in which Ser241 plays a critical catalytic role[40]. Human FAAH shares ~82% sequence identity with rat FAAH, however there are six amino acids differences within the substrate-binding pockets of hFAAH and rFAAH. To better explore the hFAAH structure in drug

design, a "humanized" rat FAAH (h/rFAAH) model was developed[41] where in the resolved h/rFAAH structure in complex with inhibitor PF-750 (2.75 Å, PDB code: 2VYA) six amino acids of the active site were mutated into those of the human FAAH protein sequence (namely Leu192Phe, Phe194Tyr, Ala377Trp, Ser435Asn, Ile491Val, and Val495Met). This discovery facilitated the design of FAAH inhibitors with equipotencies for either species, alleviating discrepancies in inhibitor activity between rodent (preclinical model) and human (clinical development). The structural insights of the resolved FAAH structures revealed the presence of three distinct channels responsible for ligand-protein interactions known as (i) the membrane access channel (MAC); (ii) the acyl-chain binding pocket (ABP); and (iii) the cytosolic port (CP).[42] This ligand-protein interaction arrangement allowed the design of FAAH inhibitors with diverse physicochemical properties (ClogP, tPSA, LipE) taking advantage of the distinct "make-up" of those regions. [30, 31] Molecular recognition of inhibition mechanism within these channels produced several series of FAAH inhibitors that interacted with the protein in a covalent or a noncovalent manner. Furthermore, the resolution of the apo structure[42] of rFAAH revealed that an open conformation is the genuine native conformation for the enzyme residue, while the closed conformation is likely triggered by the rearrangement of flexible residue side chains of the binding pocket upon ligand binding. Many designed FAAH inhibitors (Fig. 1) contain carbamate or urea pharmacophores which covalently bind to catalytic Ser241 forming a covalent carbamate adduct intermediate as an approach to achieve sustained FAAH inhibition and prolonged pharmacodynamics (PD) effects. However, this newly formed carbamate adduct, in a second phase hydrolysis process is converted back to the active enzyme, while in the process a structurally modified ligand is released as the hydrolytic product. This interconversion process "intrinsic reversibility" can be exploited by modifications of the ligand's size (length and

bulkiness) and generate analogs with "tunable" adduct residence time (τ). This unique reversible mode of FAAH inhibition represents a powerful mechanism for abrogating enzyme activity, and it is considered the most pharmacologically tractable mechanism of choice for enzyme inhibition. This strategy on targeting "covalent - reversible" drugs offers the advantage of "tuning-up" a desirable pharmacological effect of a molecular target and mimic the long-lasting activity of irreversible inhibitors, with dissociation rates *in vivo* that approach the rate of target degradation and re-synthesis.[43, 44] Also, this strategy offers an additional advantage in minimizing potential "drug-drug" interactions, since the drug could rapidly clear from the circulation (short PK effect), while still maintains a lasting target engagement effect (long PD effect). In contrast, fully irreversible adduct formation (suicidal inhibitors) have raised serious safety concerns in drug development because of the relationship between covalent drug binding and the potential of immunogenic-driven allergic reactions and idiosyncratic drug toxicity.[45, 46]

2.2 Design of new carbamate FAAH inhibitors

Our design strategy followed a traditional SAR approach and was supported by molecular modeling studies based on FAAH cocrystal structures. Examination of FAAH-inhibitor co-crystals[41, 42, 47-50] revealed that the FAAH active-site possesses high flexibility allowing several residues lining the binding cavity to attain conformations "friendly" to the interactions with structurally diverse ligands. Taking advantage of these observations, we explored carbamate FAAH inhibitors seeking compounds with high potency and selectivity with equipotency for both human- and rat-FAAH. An emphasis was given to identify new molecules with increased polarity (lower ClogP) and enhanced water solubility suitable as oral drugs. To that end, we have explored structural features based on existing FAAH templates in the literature or generated in our own lab

(Fig. 2). To support the design of new FAAH inhibitors, we have applied computational methods supported by the available X-ray crystallographic data for FAAH[41, 42, 47, 51]. To that end:

1. We have incorporated polar moieties (i.e. morpholine, dioxo-thiomorpholine) at the pharmacophoric region (C; Fig. 2) predicted to occupy the cytoplasmic channel (CP) of the binding pocket of FAAH, which represents a hydrophilic region adjacent to the catalytic site and contributes to key interactions with the polar head groups of substrates (i.e. ethanolamide moiety of AEA) and inhibitors. Those polar moieties counter the hydrophilic residues at the CP channel targeting hydrogen bonding and electrostatic interactions between ligand and protein to enhance the ligand's affinity. Even though this part of the molecule is departed upon formation of the covalent adduct between ligand-protein (carbamylation step), still it plays a critical role in forming a favorable "precovalent" pose between ligand and protein that leads to a nucleophilic attack of the catalytic Ser241 of FAAH to the carbamate moiety of the ligand to form a covalent adduct.

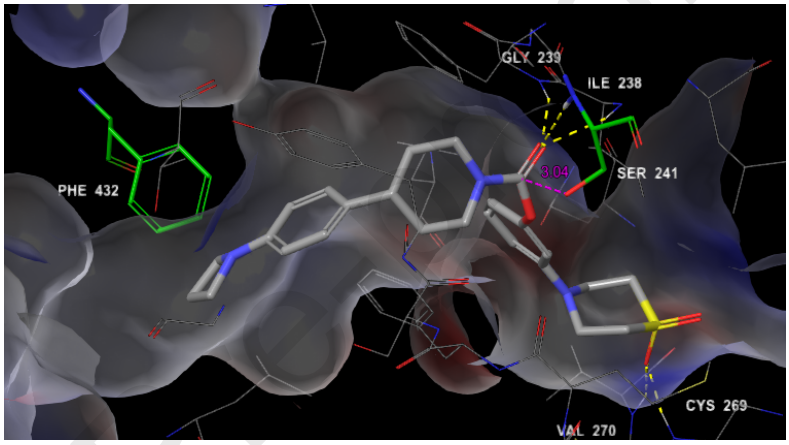

Fig. 3 Induced-fit docking of **9** with humanized FAAH crystal structure. A Connolly surface shown as electrostatic potential (red-white-blue) was used to represent the shape of the binding pocket. Catalytic residue Ser241 and Phe432, a key residue of the MAC channel, are shown in green. Key residues forming the binding pocket shown in wireframe. The ligand is shown in gray. Atoms are colored by atom type. Hydrogen bonds are indicated by yellow dashed lines, and the distance of catalytic Ser241 from the carbamate group in magenta dashed line.

2. We have added polar groups (i.e. alkoxy, cyclic-amines) at the distal aromatic region of the molecule (A; Fig. 2) predicting to occupy the ABP and MAC channels. This region of the binding pocket is primarily hydrophobic in nature, but a few residues with polar characteristics

are present at the junction of these two channels allowing polar groups of the ligand to interact favorably (i.e. hydrogen bonding) with the protein and increase ligand affinity.

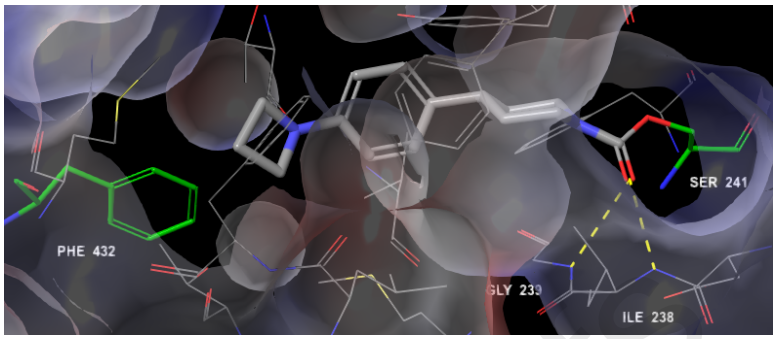

Fig. 4 Covalent docking of **9** with humanized FAAH crystal structure with the leaving group no longer attached. A Connolly surface shown as electrostatic potential (red-white-blue) was used to represent the shape of the binding pocket. Catalytic residue Ser241 and Phe432, a key residue of the MAC channel, are shown in green. Key residues forming the binding pocket shown in wireframe. The ligand is shown in gray. Atoms are colored by atom type. Hydrogen bonds are indicated by yellow dashed lines.

3. We have introduced bulky groups (i.e. substituted-, bridged-piperazines) with relative and absolute configuration as well as conformational restriction within individual analogs between the distal aromatic region and the carbamate pharmacophore (B; Fig. 2) to influence ligand selectivity and increase residence time of the newly formed covalent adducts between ligands and protein. We postulated that the bulkiness of the molecule close to the vicinity of the carbamylation adduct would retard its hydrolysis rate to restore the free enzyme (second phase hydrolysis), while prolonging the inactivation period of the enzyme and extending the pharmacodynamic effect of the drug.

2.3 Molecular modeling: Crystallographic and biochemical studies have confirmed that carbamate- or urea-based FAAH inhibitors bind covalently to catalytic Ser241 forming a carbamate adduct intermediate.[41, 42, 51, 52] However, direct structural methods assessing the binding mode of covalently bound drugs that form adducts with the protein by displacing a portion of the ligand is not practical, since the displaced group has been departed at the postcovalent state. Therefore, to gain insight of the interactions of the intact molecule with the protein to design new covalent inhibitors, we have constructed "precovalent" FAAH-ligand complexes and minimized them in the binding channel. This allowed us to pre-position the ligand within the binding pocket

of FAAH to determine if it is aligned into binding site with acceptable binding geometry. For molecules with good fit into the binding pocket, we have calculated covalent docking poses by employing Schrodinger methods. Fig. 3 illustrates the induced-fit docking of analog **9** (entry 9; Table 1) within the h/rFAAH structure (PDB code: 2VYA) in the "precovalent" state orientation, and Fig. 4 illustrates the covalent adduct formed between **9** and the catalytic Ser241 of FAAH. In the "precovalent" pose (Fig. 3), **9** orients within the FAAH binding pocket by making key hydrogen bonding interactions with residues (Ile238, Gly239, Ser241) of the CP channel, positioning the carbamate group of the ligand at a close vicinity (~ 3 Å) to the catalytic Ser241 suitable for adduct formation (carbamylation step). The azetidine ring at the distal end of the acyl chain-binding pocket is close to Phe432, a key residue of the MAC channel, which undergoes a shift toward the ABP channel expanding its regional access. The MAC channel has been suggested to serve as the "gate" for lipid substrates to enter FAAH from the cell membrane.[53] A similar ligand orientation was maintained after the covalent bond formation with the catalytic Ser241 (Fig. 4). Two key hydrogen bonding interactions between **9** and residues Ile238 and Gly239 of the CP channel are shown in Fig. 4. We have overlapped **9** and PF-3845 (Fig. 5) and found that both orient similarly within the FAAH binding pocket. During our modeling studies, we have postulated that FAAH ligands are able to effectively occupy into multiple conformations within the binding pocket to facilitate ligand adaptation for covalent bond

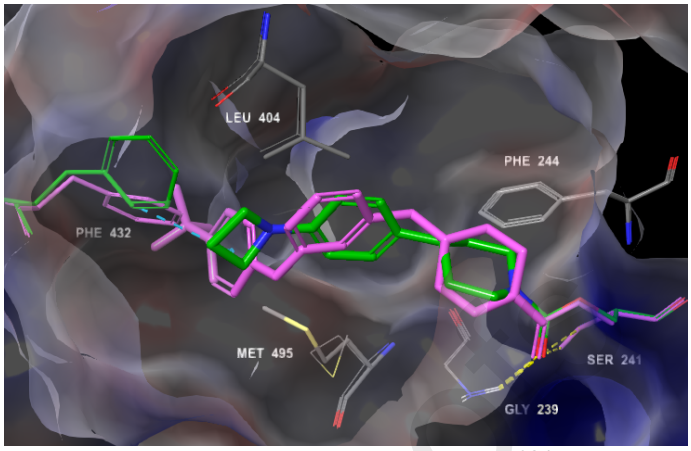

Fig. 5 Overlapped covalent docking poses of **9** (green) and **PF-3845** (magenta) with humanized FAAH crystal structure. A Connolly surface shown as electrostatic potential (red-white-blue) was used to represent the shape of the binding pocket. Phe432, a key residue of the MAC channel, is shown in green. Key residues forming the binding pocket are shown in thin tube representation (gray). Atoms are colored by atom type. Hydrogen bonds are indicated by yellow dashed lines, and π-stacking interactions shown in blue dashed lines.

formation. In support of this hypothesis, known FAAH-inhibitor cocrystal structures have revealed that the FAAH active site has remarkable flexibility, where the ABP channel is lined-up with predominately hydrophobic residues, reflecting the need of this pocket to favor nonspecific binding and keep energy wells shallow for ligand adaptation. We have routinely determined the lower energy conformations of the ligand in the absence of protein and then compared it to the low energy conformer generated during "precovalent" docking to determine structures with minimal energy penalty for synthetic consideration. Structure-activity relationship studies have produced many compounds, and in this paper, we outline selected analogs in Tables 1 and 2.

2.4 Synthesis

The compounds needed to delineate the SAR for this study were prepared according to Methods A-C.

Scheme 1

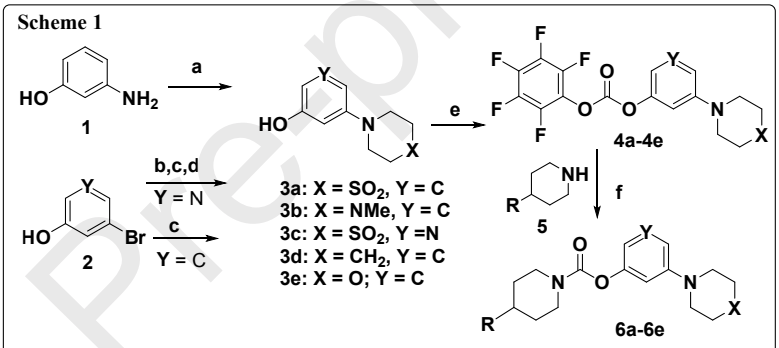

Reagents and conditions: (a) Divinyl sulfone, boric acid, glycerol (cat.), water, reflux, 3 h; (b) benzyl bromide, K_2CO_3, DMF; (c) thiomorpholine 1,1-dioxide or1-methylpiperazine, $Pd_2(dba)_3$, BINAP, NaO^{t}Bu,toluene 110 ^oC; (d) H_2, Pd/C, EtOH; (b); (e) **3** bis(pentafluorophenyl) carbonate, N,N-diisopropylethylamine, 0 ^oC to rt, 2h; (f) 4, N,N-diisopropylethylamine, 0 ^oC to rt, 2h.

2.4.1 Synthesis of piperidine analogs

Method A

The piperidine-carbamates (Table 1) were prepared according to schemes 1 and 2. Aniline **1** was treated with divinyl sulfone and boric acid to afford 4-(3-hydroxyphenyl) thiomorpholine 1,1-dioxide **3a** (**X** = SO_2, Y C)). Buchwald-Hartwig palladium cross-coupling methodology was employed to prepare phenol **3b** (**X** = NMe, **Y** = C). 3-Bromophenol was coupled with 1-

methylpiperazine in the presence of $Pd_2(dba)_3$, BINAP and NaOtBu to afford **3b.** The pyridinol **3c** (X = SO_2, **Y** =N) was prepared from 5-bromopyridin-3-ol upon protection of the hydroxyl group with benzyl bromide/potassium carbonate, followed by Buchwald-Hartwig palladium cross-coupling with thiomorpholine 1,1-dioxide and then removal of the benzyl group with H_2/ Pd/C to afford **3c**. Piperidine-phenol **3d** (**X** = CH_2, **Y** = C) and morpholine-phenol **3e** (**X** = O; **Y** = C) were commercially available. Treatment of phenols **3a-3e** with bis(pentafluorophenyl) carbonate in the presence of *N*, *N*-diisopropylethylamine produced carbonates **4a-4e**. Reaction of carbonates **4a-4e** with an appropriately substituted piperidine **5** in the presence of *N*, *N*-diisopropylethylamine afforded carbamates **6a-6e**.

Scheme 2

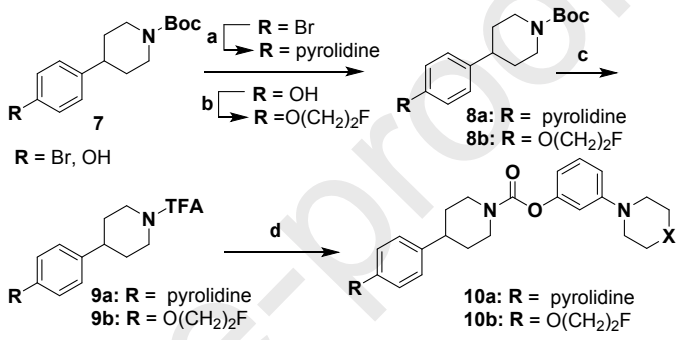

Reagents and conditions: (a) $Pd_2(dba)_3$, 2-(di-tert-butylphosphino)biphenyl, sodium tert-butoxide, pyrrolidine, toluene, 80 ^oC, 12h; (b)1-bromo-2-fluoroethane, K_2CO_3, CH_3CN, 80 ^oC, 16h; (c) TFA, CH_2Cl_2 6h, rt; (d) 3-(1,1-dioxidothiomorpholino)phenyl (perfluorophenyl) carbonate, N,N-diisopropylethylamine, 0 ^oC to rt, 2h.

Method B

Functionalization of the terminal aryl region of **7** was accomplished according to scheme 2. Aryl bromide **7** (**R** = Br) was treated with tris(dibenzylideneacetone) dipalladium(0)/2,2' bis(diphenylphosphino)-1,1'-binaphthyl and a cyclic amine (i.e. pyrrolidine) to produce aryl-piperidine **8a**. Also, alkylation of phenol **7** (**R** = OH) with an alkyl halide (i.e. 1-bromo-2-fluoroethane) in the presence of base (i.e. K_2CO_3) produced **8b (R** = OCH_2CH_2F). BOC deprotection of **8a, 8b** with trifluoroacetic acid produced amines **9a, 9b,** which were converted to final carbamates **10a, 10b** as above. (Method A).

2.4.2 Synthesis of piperazine analogs

Method C

The piperazine-carbamates (Table 2) were prepared according to scheme 3. Buchwald-Hartwig palladium cross-coupling methodology[54] was employed to prepare the aryl-piperazines **12**. Aryl halide **11** was treated with commercially BOC protected piperazines (i.e. *tert*-butyl (R)-2-methylpiperazine-1-carboxylate) or chiral substituted-piperazines to prepare analogs (**28-38**; Table 2). Tris(dibenzylideneacetone) dipalladium(0)/2,2'-bis(diphenylphosphino)-1,1'-binaphthyl was utilized as the coupling catalyst when **Y** = BOC or 2,2'-bis(diphenylphosphino)-1,1'-binaphthyl and (S)-2-methylpiperazine (BINAP when **Y** = H to afford aryl-piperazine **12**. Deprotection of the BOC group of **12** (**Y**= BOC) with trifluoroacetic acid produced amine.TFA **13**. Amine 1**3** was treated with 3-(1,1-dioxidothiomorpholino)phenyl(perfluorophenyl) carbonate **3** (scheme 1) in the presence of *N*, *N*-diisopropylethylamine to afford piperazine-carbamate **14**.

Scheme 3

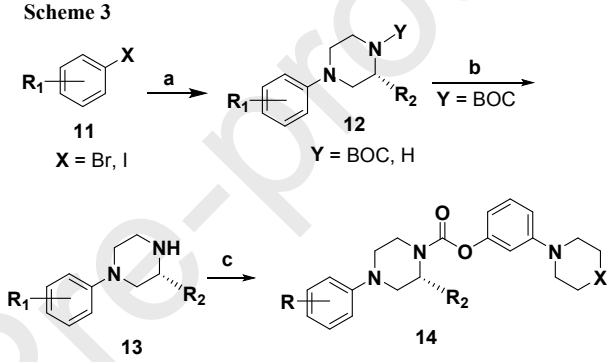

Reagents and conditions: (a) i. $Pd_2(dba)_3$, 2-(di-*tert*-butylphosphino) biphenyl, sodium *tert*-butoxide, *tert*-butyl (R)-2-methylpiperazine-1-carboxylate, 80 ^oC, 12h; ii. (R)-2-methylpiperazine toluene, 2,2'-bis(diphenylphosphino)-1,1'-binaphthyl and (S)-2-methylpiperazine, 80 ^oC, 12h; (b) TFA, CH_2Cl_2, 6h, rt; (c) 3 (scheme 1), N,N-diisopropylethylamine, 0 ^oC to rt, 2h

3. Results and Discussion

All synthesized compounds were tested for their ability to inhibit human-recombinant FAAH (hFAAH)[55] and purified rat FAAH (rFAAH)[56] using the fluorogenic substrate arachidonoyl 7-amino-4-methylcoumarin amide (AAMCA)[56, 57]. We used both species hFAAH and rFAAH to assess potential inhibitory differences, which have been previously identified by various structural chemotypes. Following similar fluorometric procedures, all compounds were also tested against hydrolytic enzymes recombinant human monoacylglycerol lipase (hMGL)[58] and human alpha/beta-hydrolase domain containing 6 (hABHD6)[59] for selectivity. Furthermore, selected compounds were evaluated for their ability to bind to CB1 and CB2 receptors using rat brain[60] or HEK293 cell membranes expressing mouse CB2 (mCB2) or human CB2 (hCB2),[61-63] respectively, via competition-equilibrium binding using [^{3}H]CP-55,940 [62-64] to minimize their involvement due to cross-reactivity of potential common pharmacophoric features.

Our design strategy was primed to optimize structural features of template shown in Fig. 2. As we discussed above, computational methods supported by available X-ray crystallographic data for FAAH and molecular modeling studies applied to pre-evaluate proposed synthetic targets. In addition, *in silico* chemoinformatics calculations (i.e., MW, LE, LipE, ClogP, and tPSA) guided the choice and priority for compounds to be synthesized to introduce desirable pharmacokinetic characteristics. Full assessment of the *in vitro* potency and selectivity as well ADME compound profiling (i.e., plasma stability, microsomal stability) was performed for selected molecules to achieve compounds with suitable druggable properties for evaluation in preclinical models of neuroprotection. A selection of compounds of our structure-activity relationship (SAR) studies are shown in Tables 1-2. We have initially sub-divided our working template (Fig. 2) into regions A to C with the ligand arranged to occupy the three distinct binging channels of FAAH.

Region A: We have identified that phenyl-dioxothiomorpholine carbamate **1** (Table 1) inhibited both species (rat, human) of FAAH at low nanomolar concentrations and displayed excellent selectivity against MGL. Computational calculations positioned the phenyl-dioxothiomorpholine moiety deep into CP channel of the binding pocket of FAAH making several key hydrogen bonding interactions and van der Waals hydrophobic contacts (i.e. Fig. 3). Keeping constant the phenyl-dioxothiomorpholine moiety, we examined the effects of the substituents at the distal phenyl moiety occupying the ABP/MAC channels of the binding pocket of FAAH. We have introduced a variety of groups at region A with polar characteristics to improve the water solubility of the parent compound and target favorable hydrogen-bonding interactions with the protein to further improve ligand affinity. Introduction of electronegative fluorine or polar alkoxy groups (entries **2**-**4**) were beneficial on improving about 2-3-fold rFAAH potency (entries **2**-**4** vs **1**). Both the fluorine nucleus and the trifluoromethoxy group were also introduced to retard any potential oxidative cytochrome P450 metabolic instability of this part of the molecule. Addition of a linear nitrile group (entry **5**) did not affect ligand affinity for rFAAH, but it decreased affinity ~3-fold for hFAAH. The longer fluoroethoxy group (entry **6**) was similar to **1** for rFAAH but showed 3-fold drop in hFAAH potency. Rotationally constraining the phenyl group of **7** by adding a methyl group at the ortho-position resulted in 2-fold drop in potency (**7** vs **1**). Next, we introduced polar amines and heterocycles (entries **8**-**13**) to further lower ClogP and improve water solubility. Amines (**8**-**10**) were similar to **1** for rFAAH, but about 2-3-fold better in hFAAH. In contrast, heterocycle pyridyl **11** and oxadiazole **12** were significantly >10-fold less potent than **1**. Addition of a hydroxyl group at the position-4 of the piperidine nucleus (**13**) also markedly reduced ligand potency (**13** vs **1**). The truncated oxetaneyl analog **14** was inactive for the target.

Region C: A significant effort was launched to examine groups positioned at the vicinity of the CP channel of FAAH's binding pocket. This part of the molecule (phenoxy-dioxothiomorpholine) departs during adduct formation, but it plays a pivotal role during the initial "preconvalent" pose of the ligand by influencing ligand adaptation within the binding pocket in a suitable orientation for the nucleophilic reaction to occur between the ligand and the catalytic residue Ser241. To that end, we have maintained the same 6-membered cyclic amine motif and altered the basicity of the group. A morpholine group (analog **15)** was similar in potency to that of the analogous dioxothiomorpholine **2**. The piperidine and piperazine analogs (**17** & **18**) showed similar potency for rFAAH with a small 3-4-fold decrease against hFAAH. To further increase the hydrophilicity of this region of the ligand, we have introduced a pyridine nucleus (entry **19),** which was well tolerated and exhibited high potency for rat and human FAAH, with IC_{50} values of 5 and 7 nM, respectively. Lastly, we have converted the carbamate pharmacophore to the analogous urea molecule **20** (**20** vs 1), since many known FAAH inhibitors carry a urea-carbamate pharmacophore (examples shown in Fig. 1). Surprisingly, the urea analog **20** was found to be inactive. This was a bit unexpected considering the close resemblance of these two scaffolds and the structural similarities they share with other reported urea-carbamate FAAH inhibitors (Fig. 1). Modeling calculations were unable to explain such a dramatic shift in FAAH potency. We postulated that the formation of a covalent adduct between the catalytic Ser241 and the urea pharmacophore of **20** didn't occur.

Table 1. Piperidine-carbamates FAAH inhibitors as neuroprotective drugs

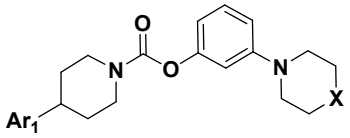

			IC_{50} nM[a]			
Compd	**Ar_1**	**X**	**rFAAH**	**hFAAH**	**hMGL**	**ClogP[c]**
1	Ph	SO2	6.0±01[b]	8.0±0.2	>1000	2.62
2	4-FPh,	SO_2	2.3±0.2	10.0±0.7	>1000	2.76
3	4-OMePh	SO_2	2.61±0.05	6.3±1.4	>1000	2.54
4	4-OCF_3Ph	SO_2	4.0±0.1	3.7±0.3	>1000	3.65
5	4-CNPh	SO_2	9.9±0.1	22.7±1.9	>1000	2.05
6	4-OCH_2CH_2F-Ph	SO_2	5.5+0.2	21.2±0.9	>1000	2.79
7	2-MePh	SO_2	10.3±1.1	15.9±1.1	>1000	3.07
8	4-N,N-dimethyl Ph	SO_2	6.9±0.3	2.4±0.4	>1000	2.78
9	4-azetidyl-Ph	SO_2	5.8±0.2	7.9±1.0	>1000	2.34
10	4-pyrrolidyl-Ph	SO_2	6.3±0.3	3.5±2.2	>1000	2.90
11	4-pyridyl	SO_2	75.5±8.1	131.6±11.1	>1000	1.12
12	3-methyl-1,2,4-oxadiazolyl	SO_2	120±6.5	147.4±11.4	>1000	0.01
13	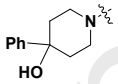	SO_2	78.1±14.3	172.2±10.3	>1000	0.98
14	oxetaneyl	SO_2	NA[d]	NA	>1000	-0.3
15	4-FPh	O	2.93±0.06	16.3±1.3	>1000	3.73
16	4-N,N-dimethyl-Ph	O	14.7±1.1	31.0±7.2	>1000	3.75
17	4-FPh	CH	6.8±0.2	40±4.2	>1000	5.10
18	4-FPh	$N\text{-}CH_3$	9.4±0.5	33.2±2.1	>1000	4.23
19	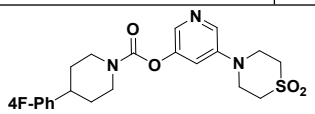		7.1±0.5	4.9±0.7	>1000	2.21
20	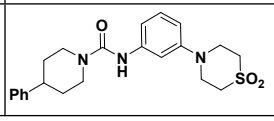		NA	NA	NA	1.75

[a] Inhibition data for h/rFAAH and hMGL were determined using throughput fluorescent assays. [b]IC_{50} ± SD values were determined from triplicate experiments. IC_{50} values were calculated using Prism software (GraphPad). [c] ClogP values were calculated using ChemDraw, version 18.2; [d]NA=not active at 1 uM.

Region B: To further expand the breadth of our SAR, we focused on region B of the molecule (Fig. 2) which potentially influences the carbamylation step between ligand and protein. This region can also affect the second phase hydrolysis of the formed adduct to regenerate the active enzyme. Piperazine **21** was almost equipotent to piperidine **1**, while piperazines **22** and **23** were a bit 3-4-fold weaker than the analogous substituted piperidines **2** and **5**. Both pyridyl and pyridazinyl analogs **24** and **25** were markedly weaker for FAAH. The more flexible benzyl analogs **26** and **27** showed good activity for both hFAAH and rFAAH with IC_{50} values of about 2 nM. Next, we introduced bulkier substituents at the piperazine moiety of relative and absolute configuration as well as conformational restriction to potentially influence both potency and ligand selectivity. Methyl substituted piperazines (**28, 29, 31, 33, 34**) were similar or better in potency for FAAH when compared to parent compound **1**. The methyl substitution displayed high enantiospecificity for FAAH, with the (R)-enantiomer being the active species (for example **29** vs **30**). Both, the dimethyl-substituted piperazine **36** and the spiro-cyclopropane **37** were weakly active at 1 uM concentration. Unpredictably, the bridged piperazines **38** and **39** were quite different with **38**-(R, R)-enantiomer being active for FAAH, while **39**-(S, S)-enantiomer was markedly 20-fold less potent. Molecular modeling studies (not shown) indicated that steric bulkiness of the ligand at region B can restrict its "preconvalent" pose alignment within the binding pocket of FAAH, and only small groups, such as methyl, with the correct conformational geometry were able to form favorable ligand poses within the binding pocket to facilitate the formation of the

covalent adduct between the ligand and the catalytic residue Ser241 of FAAH. Lastly, we synthesized piperazine-urea **40** and found to be inactive for FAAH, similarly to the urea-piperidine **20** analog.

T able 2. Piperazine carbamates FAAH inhibitors as neuroprotective drugs

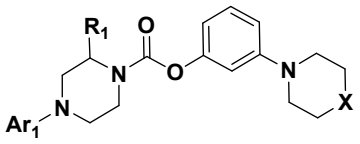

				IC$_{50}$ nM[a]			
Compd	**Ar$_1$**	**R$_1$**	**X**	**rFAAH**	**hFAAH**	**hMGL**	**ClogP[c]**
21	Ph	H	SO_2	8.0±0.1[b]	15.0±0.5	>1000	1.93
22	4-F Ph	H	SO_2	12.5±0.3	20.5±2.1	>1000	2.24
23	4-CN Ph	H	SO_2	62.7±3.5	89.3±8.3	>1000	1.76
24	2-pyridyl	H	SO_2	102.3±6.5	ND[d]	>1000	0.98
25	4-pyridazinyl	H	SO_2	NA[e]	NA	>1000	0.03
26	3-Ph-benzyl	H	SO_2	2.1±0.1	1.9±0.1	>1000	4.11
27	3-PhO-benzyl	H	SO_2	2.2±0.5	2.3±0.3	>1000	4.32
28	Ph	(RS)-Me	SO_2	5.5±0.5	2.6±0.1	>1000	2.45
29	Ph	(R)-Me	SO_2	5.7±0.2	17.7 ±3.4	>1000	2.45
30	Ph	(S)-Me	SO_2	NA	NA	ND	2.45
31	4-F Ph	(R)-Me	SO_2	6.3±0.5	11.7±2.6	>1000	2.76
32	4-F Ph	(S)-Me	SO_2	40.5±1.4	72.9±4.5	>1000	2.76
33	4-OMe	(R)-Me	SO_2	7.4±0.3	11.1±1.0	>1000	2.47
34	4-OMe	(R)-Me	O	5.2±0.9	4.1±1.8	>1000	3.43
35	4-OMe	(S)-$CHMe_2$	SO_2	NA	NA	ND	3.69
36	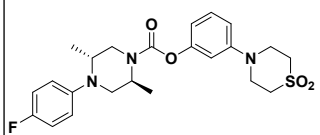			35% @ 1uM	ND	ND	3.28
37	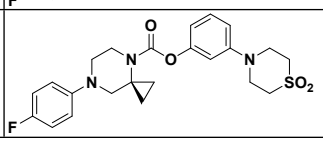			54% @	ND	ND	2.56

		1uM			
38	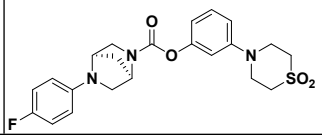	17.1±0.9	20.3±2.4	>1000	2.0
39	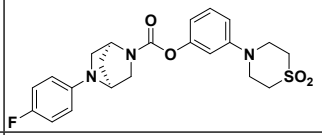	341±12	67% @ 1uM	>1000	2.0
40	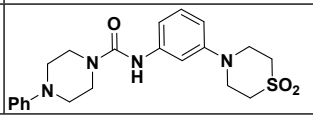	NA	NA	NA	1.29

[a] Inhibition data for h/rFAAH and hMGL were determined using throughput fluorescent assays. [b]IC_{50} ± SD values were determined from triplicate experiments. IC_{50} values were calculated using Prism software (GraphPad). [c] ClogP values were calculated using ChemDraw, version 18.2; [d]ND = not determined; [e]NA=not active at 1 uM.

4. Evaluation of FAAH inhibitors using the *in vitro* competitive activity-based protein profiling

We have assessed FAAH inhibitors **9** and **31** in the activity-based protein profiling (ABPP) assay [65] to further evaluate their selectivity. Gel-based ABPP analysis was performed using membrane homogenates prepared from rat brain tissue and the rhodamine-tagged fluorophosphonate (FP-Rh) probe that is typically used to profile the serine hydrolase superfamily[6, 51, 66]. The clinical candidate FAAH inhibitor PF04457845 was used as the positive control. Protein homogenates (10 mg/mL) were incubated with compounds **9, 31** (1 and 10 μM), **PF04457845** (10 μM) or DMSO for 30 min at room temperature. The tissues were then treated with 10 μM FP-Rh probe for 45 min at room temperature. The reaction was quenched using 2x SDS-PAGE loading buffer and separated with SDS-PAGE (12% acrylamide). Fluorescence was detected using Amersham® Imager 600 with the green epi light (520 nm) as the light source. Both inhibitors **9** and **31** completely inhibited FAAH at 1 and 10 μM without significant inhibition of other serine hydrolases. In our experiments, all

compounds appeared to share a clean selectivity profile, comparable to that of PF04457845 (Fig. 6). These ABPP studies confirmed that **9** and **31** were highly selective for FAAH in the brain, since none of the other FP-reactive serine hydrolases in this tissue were inhibited by these agents.

5. ADME Properties

We have evaluated the ADME properties of several potent (IC_{50}<10 nM) and selective (>1000-fold) carbamates FAAH inhibitors. Prepared carbamates were found to be stable ($t_{1/2}$ > 60 min) in human, rat and mouse plasma and in gastric fluids. The microsomal stability ($t_{1/2}$, min) of both classes of piperidine and piperazine carbamates in human, rat and mouse liver microsomal preparations ranged between 15 to 25 min, with human microsomal preparations being the most stable species. We have also evaluated several carbamates in cassette pharmacokinetics experiments (dose: 2 mg/kg, iv, at 15 min) to rank-order them for brain penetrability.

Based on the findings (Table 3), the tested analogs were brain permeable by comparing brain and plasma levels after iv administration at 15 min.

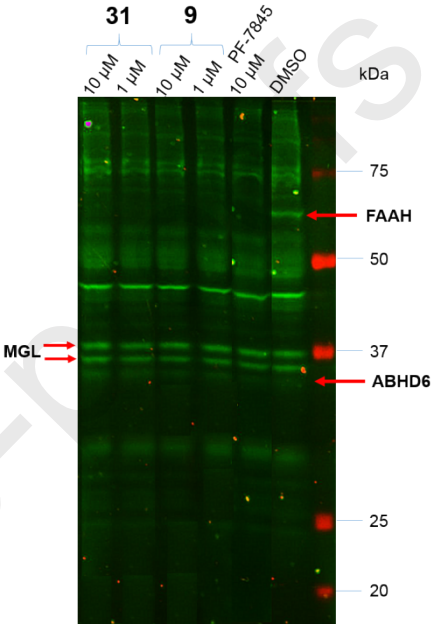

Figure 6. Gel-based ABPP analysis was performed using membrane homogenates prepared from rat brain tissue and the rhodamine-tagged fluorophosphonate (FP-Rh) probe. FAAH inhibitors **9** and **31** completely inhibited FAAH at 1 and 10 µM without significant inhibition of other serine hydrolases. Representative additional brain serine hydrolases are designated based on previous ABPP studies[6].

Table 3. Cassette pharmacokinetics experiments of brain permeability

Compd	**2**	**15**	**8**	**6**
15 min IV brain (µg/mL)	1.23 ± 0.18	0.508 ± 0.034	1.11 ± 0.21	0.909 ± 0.158
15 min IV plasma (µg/mL)	0.474 ± 0.066	0.506 ± 0.056	0.746 ± 0.121	0.388 ± 0.062
Cassette pharmacokinetics at 2 mg/kg, iv. The compounds were brain permeable by comparing brain and plasma levels after iv administration at 15 min.				

6. Pharmacology

Excitotoxic damage can occur from epilepsy and other seizure disorders, stroke, birth trauma, traumatic brain injury, fever (especially in children), genetic conditions, and exposure to convulsive environmental toxins and nerve agents. Effective treatments must be administered immediately or several hours after an excitotoxic insult to reduce brain deterioration and cognitive defects, the latter correlating best with synaptic decline in many disorders[67, 68]. FAAH inhibitors represent an advantageous pharmacological approach of modulating repair signaling linked to the "on-demand action" of endocannabinoids that are elevated in response to neurodegenerative insults. We tested inhibitors **9** and **31** for their neuroprotective ability by assessing synaptic markers known to be vulnerable to excitotoxic insults in the hippocampal slice models[14, 69, 70] as well as in different *in vivo* models of excitotoxicity and related seizure induction[71-73]. Hippocampal slice cultures prepared from rats at postnatal days 12 and 13 were used for the experiments. The cultured slices express compensatory responses to injury and survival signaling pathways that are similar to those found in the adult brain. To monitor protection by the carbamate inhibitors, we applied particular focus on an AMPA receptor subunit (GluR1) as a vulnerable synaptic component in the KA insult slice model since previous studies found reductions and altered functionality of AMPA receptor measures correlating with seizure effects after KA

exposure[69, 71, 74] and after soman-induced seizures[72]. The KA insult caused significant reductions

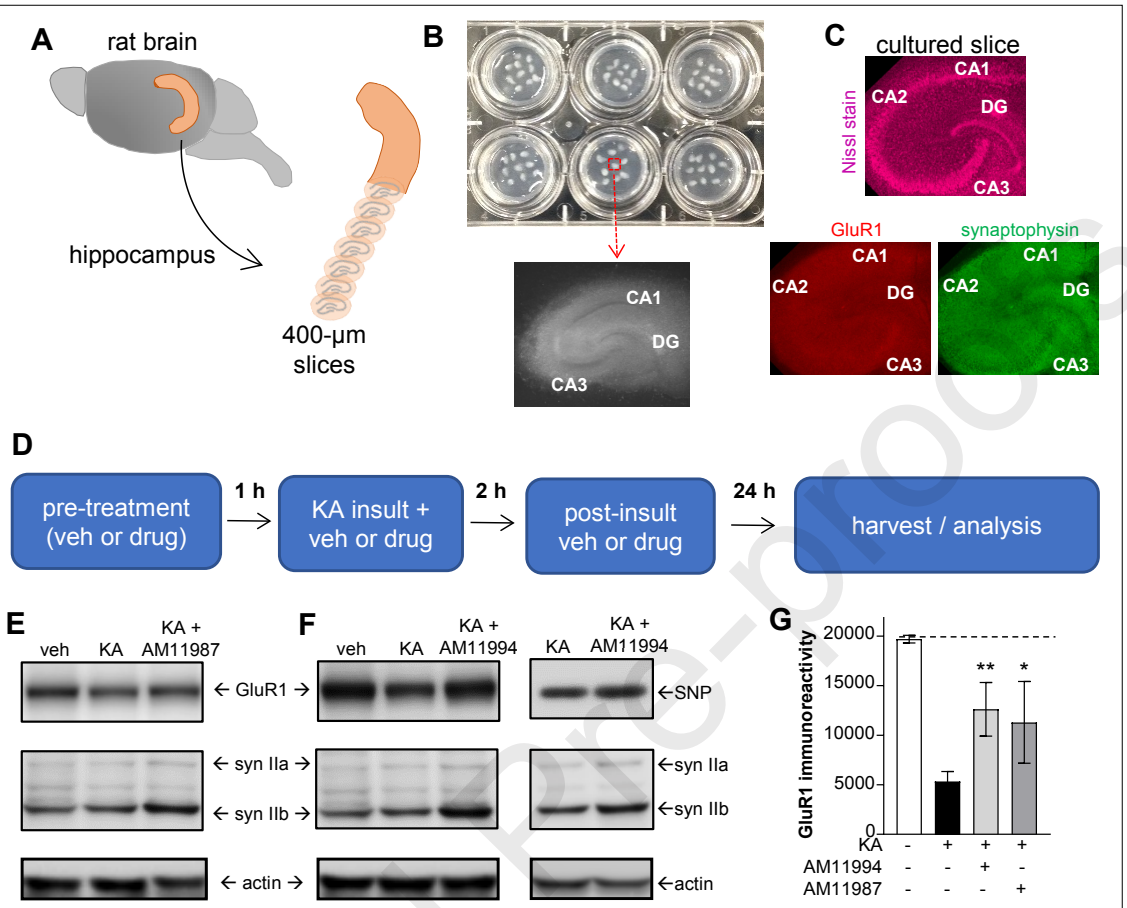

Figure 7. Synaptic protection mediated by FAAH inhibitors in the hippocampal slice model of kainic acid (KA)-induced excitotoxicity. Hippocampal tissue from 12-day-old rats was removed and transverse slices of 400-µm thickness prepared (A), the slices being maintained in six-well culture plates and exhibiting intact neuronal subfields (B). Stable neuronal density determined by Nissl as well as pre- and postsynaptic marker staining was consistently found after several weeks in culture (C, width of view-fields: 1.5 mm). The experimental design includes control slices treated with vehicle only, as well as a 1-h pre-treatment step with vehicle (veh, 0.01% DMSO), FAAH inhibitor compound 9 (AM11994), or compound 31 (AM11987) before a 2-h KA insult with continued presence of vehicle or inhibitor (D). After washout of KA, the cultured slices were incubated with vehicle or FAAH inhibitor for 24 h, followed by harvesting of the brain tissue for subsequent analyses. In order to evaluate potential synaptic protection by compounds 31 (E) and 9 (F), equal protein aliquots of homogenized samples from the different treatment groups were assessed by immunoblot for GluR1, synapsin IIa and IIb (syn IIa and IIb), synaptophysin (SNP), and actin. Integrated optical density measures for GluR1 are shown as means ± SEM (G). Unpaired t-tests compared to KA insult alone: **p<0.01 (two-tailed), *p=0.0292 (one-tailed).

in the postsynaptic AMPA receptor subunit GluR1 and in the synaptic vesicle-associated synapsin IIa and synapsin IIb. Rat hippocampal slice cultures were pre-treated with FAAH inhibitor or with vehicle (0.1% DMSO) for 1 h. The cultures then were subjected to control treatment (NT) or to an

excitotoxic insult with 60 μM kainic acid (KA) for 2 h in the presence of vehicle or the corresponding FAAH inhibitors used for the pre-treatments. After a washout step, the cultured slices were then incubated with vehicle or correspondence FAAH inhibitor for 24 h. Then, slices

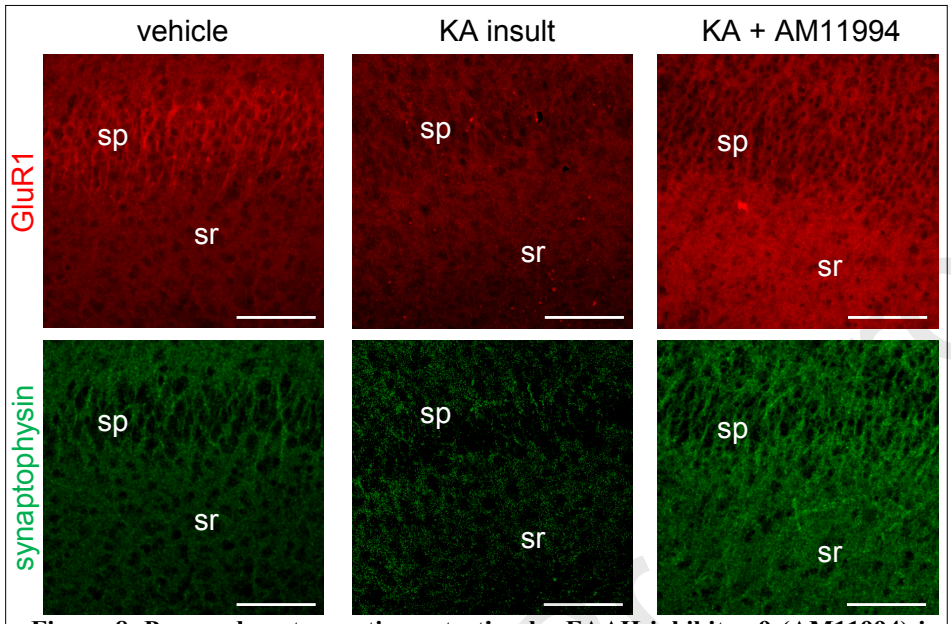

Figure 8. Pre- and postsynaptic protection by FAAH inhibitor 9 (AM11994) in the excitotoxic hippocampal slice. Mature slice cultures were treated with vehicle only, or pre-treated with vehicle or FAAH inhibitor compound **9** (AM11994) for 1 h before the 2-h KA insult step. After washout of KA, slices were incubated with vehicle or compound **9** for the 24-h post-insult period, then fixed and double immunostained with anti-GluR1 (red) and anti-synaptophysin (green). Size bars: 100 μm. DG, dentate gyrus; sp, stratum pyramidale; sr, stratum radiatum.

were harvested into groups of 7-9, sonicated, and equal protein aliquots assessed for AMPA receptor subunit GluR1, synaptophysin, and synapsin IIb by immunoblot (Fig. 7). FAAH inhibitors afforded neuronal protection in the hippocampus after KA-induced excitotoxicity with **9** as well as with **31**. Pre- and postsynaptic protection was evident in the dense neuropil of the hippocampal subfield CA1 (Fig. 8). Due to the protective results produced by **9** in the slice model, it is noteworthy that initial *in vivo* studies were conducted with **9** to assess its effects on KA-induced seizures, and preliminary results found an expected reduction in seizure severity scores (unpublished observation).

7. Conclusions

We have discovered new series of potent and selective carbamate FAAH inhibitors. FAAH is an enzyme implicated in the hydrolysis of endocannabinoid *N*-arachidonoylethanolamine (AEA) which is a partial agonist of CB1 receptors. CB1 receptor activation reduces excessive glutamatergic signaling and excitotoxic progression, thereby protecting hippocampal cells from cytoskeletal and synaptic damage. FAAH inhibitors offer safety advantages by augmenting the anandamide levels "on demand" to promote CB1 protective neuroprotective mechanisms without the adverse psychotropic effects usually seen with direct and chronic activation of the CB1 receptor. The new inhibitors showed potent nanomolar inhibitory activity against recombinant human and purified rat FAAH, and were selective (>1000-fold) against serine hydrolases MGL and ABHD6, while lacked of any affinity for the cannabinoid receptors CB1 and CB2. Evaluation of FAAH inhibitors **9** and **31** using the *in vitro* competitive activity-based protein profiling (ABPP) assay confirmed that both inhibitors were highly selective for FAAH in the brain, since none of the other FP-reactive serine hydrolases in this tissue were inhibited by these agents.

Our design strategy followed a traditional SAR approach and was supported by molecular modeling studies based on FAAH cocrystal structures. To rationally design new molecules that are irreversibly bound to FAAH, we have constructed "precovalent" FAAH-ligand complexes to identify good ligand binding geometries within the binding pocket of FAAH and then calculated covalent docking poses by employing Schrodinger methods to select compounds for synthesis. FAAH inhibitors **9** and **31** were evaluated for neuroprotection in rat hippocampal slice cultures. In the brain tissue, both inhibitors displayed protection against synaptic deterioration produced by kainic acid-induced excitotoxicity. Thus, the resultant compounds produced through rational

design are providing early leads for developing therapeutics against seizure-related damage associated with a variety of disorders.

7. Supplementary data

Experimental details for the preparation of all compounds described in Tables 1 and 2 have been provided.

Acknowledgments. The authors thank Heather Romine and Matthew Montilus for excellent assistance. This work was supported by the Alzheimer's Drug Discovery Foundation (ADDF), Boston, MA [grant number ADDF # 20150503].

8. Experimental Section

8.1 Chemistry

Proton nuclear magnetic resonance spectra were obtained on a VARIAN 400 spectrometer at 500 MHz. Spectra are given in ppm (δ) and coupling constants, *J* values, are reported in hertz. Splitting patterns are designated as follows: s, singlet; brs, broad singlet; d, doublet; t, triplet; q, quartet; m, multiplet. Tetramethylsilane was used as an internal reference standard. Mass spectra were obtained on a Waters Micromass ZQ spectrometer. HPLC techniques and high-resolution mass spectrometry were used to determine compound purity. All reagents and solvents were obtained from commercial suppliers and used without further purification. All non-aqueous reactions were carried out in oven-dried glassware under an atmosphere of dried argon or nitrogen. The reactions were monitored by thin layer chromatography (TLC plates F254, Merck) or LC-MS analysis. All

products, unless otherwise noted, were purified by flash chromatography using a Biotage Isolera purification system with pre-packed silica cartridges. Purity of all final products was > 96% as determined by LC-MS using the following protocol. Mobile Phase A = water, B = acetonitrile solvent gradient 95/5 to 5/95 A:B in 11 min; flow rate 1.5 mL/min; Waters XTerra MS C8 column (4.6 × 50 mm) with UV detection at 190-400 nm wavelength. The following abbreviations are used: $CDCl_3$, deuterated chloroform; EtOAc, ethyl acetate; CH_2Cl_2, dichlorometane; $MgSO_4$, magnesium sulfate; THF, tetrahydrofuran; NH_4Cl, ammonium chloride; MeOH, methanol; $NaHCO_3$, sodium bicarbonate; TFA, trifluoroacetic acid; LC-MS, liquid chromatography with mass spectrometry; MS, mass spectrometry; NMR, nuclear magnetic resonance spectrometry; TLC, thin layer chromatography.

Method A (Scheme 1)

8.1.1 4-(3-hydroxyphenyl)thiomorpholine 1,1-dioxide (4; X = SO_2)

Step a) Water (30 mL), boric acid (30 mol %), and glycerol (6 drops) were added to a stirred solution of 3-amino phenol **1** (3.2 g, 29.32 mmol) and divinyl sulfone (3.46 g, 29.32 mmol) and the mixture was refluxed for 3 h. Then, the reaction mixture was extracted with ethyl acetate, and the organic layer was washed three times with water and dried over $MgSO_4$. The solvents were removed under vacuum and the crude product was washed with hot petroleum ether to give 4-(3-hydroxyphenyl)thiomorpholine 1,1-dioxide 6.21 g, as white solid. ^{1}H NMR (500 M Hz, *$CDCl_3$*) δ 7.26 (t, 1H, *J* = 8.0 Hz); 6.48 (dd, 1H, *J* = 8.0 Hz, *J* = 2.5 Hz); 6.40-6.37 (m, 3H); 5.15 (bs, 1H,); 3.85 (t, 2H, *J* = 5.0 Hz); 3.08 (t, 2H, *J* = 5.0 Hz).

8.1.2 3-(Benzyloxy)-5-bromopyridine

Step b) Potassium carbonate (1.38 g, 10 mmol) was added to a stirred solution of 5-bromopyridin-3-ol (0.860 g, 5 mmol) in DMF (20 mL). Benzyl bromide (1.28 g, 1.43 mL, 7.5 mmol) was added and the resulting reaction mixture was stirred at 80 °C for 6 hours. The reaction mixture was cooled to room temperature and partitioned between diethyl ether (100 mL) and water (50 mL). The organic phase was separated, dried over Na_2SO_4 and evaporated. The residue was purified by flash chromatography on silica (Biotage; eluting solvents Hex: EtOAc 1/2 ratio) (1.06 g, 80% yield). ^{1}H NMR (500 MHz, *$CDCl_3$*) δ 8.30 (dd, J=4.4, 2.4 Hz, 2H), 7.45-7.33 (m, 6H), 5.08 (s, 2H).

8.1.3 4-(5-(Benzyloxy)pyridin-3-yl)thiomorpholine 1,1-dioxide

Step c). To a stirred solution of *3-(benzyloxy)-5-bromopyridine* (1 g, 3.7 mmol) in toluene (25 mL), were added tris(dibenzylideneacetone)dipalladium(0) (169 mg, 0.185 mmol), 2,2'-bis(diphenylphosphino)-1,1'-binaphthyl (230 mg, 0.37 mmol) and sodium *tert*-butoxide (710 mg, 7.4) and the flask was purged with argon. Thiomorpholine 1,1-dioxide (766 mg, 5.68) was added to the mixture and heated to 80 ^{o}C for 14 hours. After the completion of the reaction (monitored by TLC) the solvent was removed under vacuum. Water was added (10 mL) and the mixture was extracted with ethyl acetate (3x30 mL). The combined organic layer was dried over Na_2SO_4 and concentrated under reduced pressure. The residue was purified on silica gel (Biotage; eluting solvents DCM: MeOH 10/1 ratio) to obtain red oil (720 mg, 60% yield); ^{1}H NMR (500 MHz, *$CDCl_3$*) δ 7.96 (m, 2H), 7.41-7.34 (m, 5H), 6.75 (t, J = 2.2 Hz, 1H), 5.10 (s, 2H), 3.85 – 3.83 (m, 4H), 3.08 – 3.06 (m, 4H).

8.1.4 4-(5-Hydroxypyridin-3-yl)thiomorpholine 1,1-dioxide (3; X = SO_2, Y = N)

Step d). 10% Palladium-carbon (50 mg) was added to an ethanol (20 ml) solution containing 4-(5-(benzyloxy)pyridin-3-yl)thiomorpholine 1,1-dioxide (500 mg), The resulting reaction mixture was stirred at room temperature in presence H_2 atmosphere for 24 hours. The reaction mixture was filtered through celite bed the bed was washed with ethanol. The filtrate was concentrated under reduced pressure to afford 4-(5-hydroxypyridin-3-yl)thiomorpholine 1,1-dioxide as colorless liquid (350 mg, 98% yield); ^{1}H NMR (500 MHz, *CDCl$_3$*) δ 7.87 (d, *J* = 1.9 Hz, 1H), 7.79 (d, *J* = 2.3 Hz, 1H), 6.93 (d, *J* = 2.1 Hz, 4H), 3.83 (d, *J* = 4.8 Hz, 18H), 3.09 – 3.05 (m, 4H).

8.1.5 Morpholinophenyl (perfluorophenyl) carbonate (3; X = O; Y = C)

It was prepared according to step d) from 3-bromophenol and 1-methylpiperazine in the presence of $Pd_2(dba)_3$, BINAP and NaOtBu. ^{1}H NMR (500 MHz, *CDCl$_3$*) δ 7.29-7.24 (m, 2H),) 6.83-6.81 (m, 1H), 6.77-6.75 (m, 2H), 3.86-3.84 (m, 4H), 3.19-3.17 (m, 4H).

8.1.6 3-(1,1-Dioxidothiomorpholino)phenyl (perfluorophenyl) carbonate (3; X = SO$_2$)

Step e). To a cold (0 ^{o}C) solution of 4-(3-hydroxyphenyl)thiomorpholine 1,1-dioxide (227 mg, 1 mmol), and *N*, *N*-diisopropylethylamine (0.26 mL, 1.5 mmol) in dichloromethane (15 mL) was added bis(pentafluorophenyl) carbonate (433 mg, 1.1 mmol). The reaction mixture was gradually allowed to come to room temperature and stirred for 2 h. Then, the reaction was diluted in dichloromethane (25 mL) and washed with water and brine. The organic extracts were dried over anhydrous Na_2SO_4. The solvents were removed under vacuum and the residue was purified on silica gel (Biotage; eluting solvents hexanes: EtOAc 4/1 ratio) to afford 3-(1,1-dioxidothiomorpholino)phenyl (perfluorophenyl) carbonate as colorless solid (400 mg, 91%

yield). ^{1}H NMR (500 MHz, *CDCl$_3$*) δ 7.37-7.33 (m, 1H),6.86-6.80 (m, 3H), 3.90-3.87 (m, 4H), 3.12-3.10 (m, 4H).

8.1.7 3-(1,1-Dioxidothiomorpholino)phenyl 4-(4-fluorophenyl)piperidine-1-carboxylate (4; R = 4F-phenyl; compound 2, Table 1)

Step f). To a cold (0 ^{o}C) solution of 4-(4-fluorophenyl)piperidine (89 mg, 0.5 mmol) and *N*, *N*-diisopropylethylamine (174 mg, 1 mmol) in dichloromethane (5 mL) was added dioxidothiomorpholino)phenyl (perfluorophenyl) carbonate (3; **X** = SO_2, 240 mg, 0.55 mmol). The reaction mixture was gradually allowed to come to room temperature and stirred for 2 h. Then, the reaction was diluted in dichloromethane (15 mL) and washed with water and brine. The organic extracts were dried over anhydrous Na_2SO_4. The solvents were removed under vacuum and the residue was purified on silica gel (Biotage; eluting solvents hexanes: EtOAc 1/1 ratio) to afford 3-(1,1-dioxidothiomorpholino)phenyl 4-(4-fluorophenyl)piperidine-1-carboxylate as colorless liquid (150 mg, 70% yield). ^{1}H NMR (500 MHz, *CDCl$_3$*) δ 7.27-7.22 (m, 1H), 7.17 (dd, *J* = 8.5, 5.4 Hz, 2H), 7.00 (t, *J* = 8.7 Hz, 2H), 6.73 (dd, *J* = 8.3, 1.5 Hz, 1H), 6.68 (dd, *J* = 3.9, 1.7 Hz, 2H), 4.38 (d, *J* = 13.7 Hz, 2H), 3.91-3.77 (m, 4H), 3.15 – 3.00 (m, 5H), 2.92 (t, *J* = 12.2 Hz, 1H), 2.71 (ddd, *J* = 12.2, 8.8, 3.4 Hz, 1H), 1.89 (d, *J* = 13.3 Hz, 2H), 1.69 (qd, *J* = 12.8, 4.3 Hz, 2H); MS (ES) m/z 433.6017 $[M+1]^+$; purity 100%, retention time 4.70 min.

Method B (scheme 2)

8.1.8 Tert-butyl 4-(4-(pyrrolidin-1-yl)phenyl)piperidine-1-carboxylate (8a; R = pyrrolidine)

Step a). To a stirred solution of *tert*-butyl 4-(4-bromophenyl)piperidine-1-carboxylate (170 mg, 0.5 mmol) in toluene (5 mL), were added tris(dibenzylideneacetone)dipalladium(0) (46 mg, 0.05 mmol), 2,2'-bis(diphenylphosphino)-1,1'-binaphthyl (62 mg, 0.1 mmol) and sodium *tert*-butoxide (96 mg, 2 mmol) and the flask was purged with argon. Pyrrolidine (71 mg, 1 mmol) was added to the mixture and heated to 80 ^{o}C for 12 hours. After the completion of the reaction (monitored by TLC) the solvent was removed under vacuum. Water was added (10 mL) and the mixture was extracted with ethyl acetate (3x30 mL). The combined organic layer was dried over Na_2SO_4 and concentrated under reduced pressure. The residue was purified on silica gel (Biotage; eluting solvents hexane: EtOAc 10/1 ratio) to give *tert*-butyl 4-(4-(pyrrolidin-1-yl)phenyl)piperidine-1-carboxylate as colorless liquid (100 mg, 60 % yield).

8.1.9 Tert-butyl 4-(4-(2-fluoroethoxy)phenyl)piperidine-1-carboxylate (8b, R = OCH_2CH_2F)

Step b). To a stirred solution of *tert*-butyl 4-(4-hydroxyphenyl)piperidine-1-carboxylate (100 mg, 0.36 mmol) in MeCN (10 mL) was added 1-bromo-2-fluoroethane (91 mg, 0.72 mmol) and potassium carbonate (100 mg, 0.72 mmol). The reaction was stirred at 80 °C for 16 hours. The reaction mixture was diluted with water (10 mL) and extracted with dichloromethane (3x20 mL). The organic layer was dried over Na_2SO_4, filtered and evaporated to afford *tert*-butyl 4-(4-(2-fluoroethoxy)phenyl)piperidine-1-carboxylate as colorless liquid. (95 mg, 82% yield). ^{1}H NMR (500 MHz, *$CDCl_3$*) δ 7.12 (d, *J* = 8.4 Hz, 2H), 6.87 (d, J = 8.8 Hz, 2H), 4.81-4.78 (m, 1H), 4.69-4.67 (m, 1H), 4.24-4.17 (m, 3H), 2.82-2.75 (m, 2H), 2.62-2.56 (m, 1H), 1.81-1.78 (m, 2H), 1.62-1.57 (m, 3H), 1.48 (s, 9H).

8.1.10 4-(4-(2-Fluoroethoxy)phenyl)piperidine• TFA salt (9b; R = OCH_2CH_2F)

Step c). To a cold (0 °C) solution of tert-butyl 4-(4-(2-fluoroethoxy)phenyl)piperidine-1-carboxylate (100 mg, 0.30 mmol) and dichloromethane (15 mL) was slowly added trifluoroacetic acid (0.15 mL, 1.5 mmol). The resulting reaction mixture was stirred at room temperature for 6 hours. The mixture was concentrated in vacuum to afford 4-(4-(2-fluoroethoxy)phenyl)piperidine • TFA salt which was used in the next step without further purification.

8.1.11 3-(1,1-Dioxidothiomorpholino)phenyl 4-(4-(2-fluoroethoxy)phenyl)piperidine-1-carboxylate (10b; R = OCH_2CH_2F; compound 6 Table 1).

Step d). This step was performed according to Method A.

^{1}H NMR (400 MHz, *$CDCl_3$*) δ 7.29-7.25 (m, 1H), 7.16-7.12 (m, 2H), 6.90 (d, *J* = 8.6 Hz, 6H), 6.75-6.69 (m, 2H), 4.81 – 4.79 (m, 1H), 4.70-4.67 (m, 1H), 4.40 (s, 2H), 4.25-4.23 (m, 1H), 4.18-4.16 (m, 1H), 3.86-3.82 (m, 4H), 3.11-3.06 (m, 4H), 2.95-2.93 (m, 1H), 2.72-2.66 (m, 1H), 1.91 (d, *J* = 13.1 Hz, 2H), 1.76-1.75 (m, 3H). MS (ES) m/z 476.1781 $[M+1]^+$.

Method C (scheme 3)

8.1.12 Tert-butyl (R)-4-(4-methoxyphenyl)-2-methylpiperazine-1-carboxylate (12; R_1 = OMe, R_2 = (R)-Me

Step a). To a stirred solution of 1-bromo-4-methoxybenzene (187 mg, 1 mmol) in toluene (5 mL), were added tris(dibenzylideneacetone)dipalladium(0) (91 mg, 0.1 mmol), 2,2'-bis(diphenylphosphino) -1,1'-binaphthyl (124 mg, 0.2 mmol) and sodium *tert*-butoxide (192 mg, 2 mmol) and the flask was purged with argon. Then, *tert*-butyl (R)-2-methylpiperazine-1-carboxylate (150 mg, 1.5 mmol) was added to the mixture and heated to 80 °C for 12 hours. After

the completion of the reaction (monitored by TLC) the solvent was removed under vacuum, and water was added (10 mL). The mixture was extracted with ethyl acetate (3x30 mL). The combined organic layer was dried over Na_2SO_4 and concentrated under reduced pressure and the residue was purified on silica gel (Biotage; eluting solvents hexane: EtOAc 10/1 ratio) to give *tert*-butyl (R)-4-(4-methoxyphenyl)-2-methylpiperazine-1-carboxylate as colorless liquid (220 mg, 71% yield). ^{1}H NMR (500 MHz, *CDCl$_3$*) δ 6.84 (q, *J* = 9.0 Hz, 4H), 4.31 (s, 1H), 3.92 (d, *J* = 13.1 Hz, 1H), 3.75 (s, 3H), 3.31 (d, *J* = 11.5 Hz, 1H), 3.24 – 3.18 (m, 2H), 2.80 (dd, *J* = 11.7, 3.7 Hz, 1H), 2.63 (td, *J* = 11.8, 3.4 Hz, 1H), 1.47 (s, 9H), 1.30 (d, *J* = 6.7 Hz, 3H).

8.1.13 (R)-1-(4-methoxyphenyl)-3-methylpiperazine• TFA salt (13; R_1 = OMe; R_2 = (R)-Me)

Step b). Trifluoroacetic acid (0.25 mL, 3.26) was slowly added to a cold (0 ^{o}C) solution of *tert*-butyl (R)-2-methylpiperazine-1-carboxylate (200 mg, 0.65 mmol) and dichloromethane (15 mL). The resulting reaction mixture was stirred at room temperature for 6 hours and concentrated in vacuum to afford (R)-1-(4-methoxyphenyl)-3-methylpiperazine • TFA, which was used in the next step without further purification.

8.1.14 3-(1,1-Dioxidothiomorpholino)phenyl (R)-4-(4-methoxyphenyl)-2-methylpiperazine-1-carboxylate (14; R_1 = OMe; R_2 = (R)-Me, compound 32, Table 2)

Step c). 3-(1,1-Dioxidothiomorpholino)phenyl (perfluorophenyl) carbonate (75 mg, 0.17 mmol) was added to a cold 0 ^{o}C solution of (R)-1-(4-methoxyphenyl)-3-methylpiperazine• TFA (50 mg, 0.156 mmol), and N,N-diisopropylethylamine (0.14 mL, 0.78 mmol in dichloromethane (3 mL). The reaction mixture was gradually allowed to come to room temperature and stirred for 2 h. Then, the reaction was diluted in dichloromethane (15 mL) and washed with water (2 x 15 mL) and brine.

The organic extracts were dried over anhydrous Na_2SO_4. The solvents were removed under vacuum and the residue was purified on silica gel (Biotage; eluting solvents hexanes: EtOAc 1/1 ratio) to afford 3-(1,1-dioxidothiomorpholino)phenyl (R)-4-(4-methoxyphenyl)-2-methylpiperazine-1-carboxylate (50 mg, 70% yield). ^{1}H NMR (500 MHz, *CDCl$_3$*) δ 7.28-7.26 (m, 1H), 6.87 (dd, *J* = 23.5, 9.1 Hz, 4H), 6.73 (d, *J* = 8.4 Hz, 1H), 6.70-6.64 (m, 2H), 4.50 (s, 1H), 3.85 – 3.83 (m, 4H), 3.76 (s, 3H), 3.40 (d, *J* = 11.2 Hz, 2H), 3.26 (d, *J* = 11.8 Hz, 1H), 3.09 – 3.07 (m, 4H), 2.93 (dd, *J* = 11.6, 3.1 Hz, 1H), 2.75 (td, *J* = 11.9, 3.2 Hz, 1H), 1.45 (d, *J* = 5.8 Hz, 3H). MS (ES) m/z 460.6300 $[M+1]^+$; purity 100%, retention time 4.59 min.

8.1.15 N-(3-(1,1-dioxidothiomorpholino)phenyl)-4-phenylpiperazine-1-carboxamide (40)

A solution of phenyl piperazine (0.6 g, 3.69 mmol) and phenyl (3-(1,1-dioxidothiomorpholino)phenyl) carbamate (1.28 g, 3.69 mmol) in acetonitrile was heated in a sealed tube under microwave irradiation at 120 ^{o}C for 10 min with stirring. The reaction mixture was cooled to room temperature and solvent was removed under reduced pressure. The crude material was partitioned between dichloromethane and water. The aqueous phase was extracted with dichloromethane. The combined extracts were dried over $MgSO_4$ and concentrated. Chromatography of the residue gave 1.28 g of N-(3-(1,1-dioxidothiomorpholino)phenyl)-4-phenylpiperazine-1-carboxamide as white solid.

^{1}H NMR (500 M Hz, *CDCl$_3$*) δ 7.31 (t, 2H, *J* = 8 Hz); 7.25-7.19 (m, 3H); 7.06 (t, 1H, *J* = 8 Hz); 6.98 (bs, 1H); 6.68 (bs, 1H), 6.48 (d, 1H, *J* = 7.5 Hz); 4.24 (t, 4H, *J* = 5.0 Hz); 3.65 (t, 4H, *J* = 5 Hz); 3.37 (t, 2H, *J* = 5 Hz); 3.17 (t, 2H, *J* = 5 Hz); 2.96 (t, 2H, *J* = 8 Hz); 2.70 (t, 2H, *J* = 8 Hz); MS (ES) m/z 415.1855 $[M+1]^+$.

9. Pharmacology methods

9.1 Hippocampal slice cultures. Sprague-Dawley rat litters (Charles River Laboratories, Wilmington, MA) were housed and maintained in accordance with the recommendations from the Guide for the Care and Use of Laboratory Animals from the National Institutes of Health, and in accordance with an approved protocol from the Institutional Animal Care and Use Committee of the University of North Carolina-Pembroke. Brain tissue from postnatal 12-day-old was rapidly removed to prepare hippocampal slices as performed previously[14, 75, 76]. Transverse hippocampal slices (400 μm thickness) were immediately placed in ice-cooled-buffer solution (pH 7.2) then transferred in groups of eight to nine onto the Biopore membrane of Millicell-CM culture inserts (Millipore, Billerica, MA). The media below the culture inserts contained 50% basal medium eagle (Sigma-Aldrich, St. Louis, MO), 25% Earle's balanced salts (Sigma-Aldrich), 25% horse serum (Gemini Bio-Products, Sacramento, CA), and defined supplements as previously described[75, 76]. The hippocampal slices were kept in a 5% CO_2-enriched atmosphere which was maintained at 37°C, and the slices were allowed to mature for 18-20 days prior to culture treatments.

9.2 To test neuroprotection against excitotoxic insult in vitro. The FAAH inhibitors **9** and **31** were synthesized at Northeastern University (Boston, MA). Both inhibitors were initially prepared at 30 mM in dimethyl sulfoxide (DMSO). The excitotoxic insult was performed using kainic acid (KA, Tocris, Ellisville, MO) initially prepared in serum-free media. Hippocampal slice cultures were pretreated with either 3-30 μM of FAAH inhibitor **9** or **31** at a final DMSO concentration of 0.1%, and the same DMSO level in serum-free media was supplied to vehicle control slices. After the 60-min pretreatment, the media were removed and 60 μM KA was applied to the slices for 2 h in the absence or presence of the FAAH inhibitors or vehicle. After the 2-h excitotoxic insult

period, all slice cultures were gently subjected to three washout steps in order to remove the KA, thus allowing for a KA-free recovery period of 24 h with 30 μM of the respective FAAH inhibitors or vehicle. Subsequently, the brain explants were harvested into groups of 7-9, sonicated, and equal protein aliquots assessed for AMPA receptor subunit GluR1 (1:1,000, Millipore), synaptophysin (1:1,000, Abcam, Cambridge, MA), and synapsin IIb (1:1,000, Abcam) by immunoblot as previously described[76]. The GluR1 stained antigens were scanned at high resolution to determine integrated optical density measures using the imager software, and the immunoreactivity level was plotted and tested with two-tailed unpaired t-tests using Prism software (GraphPad, San Diego, CA). Additionally, fixed hippocampal tissue from each treatment group were immunostained with anti-GluR1 (1:200, Millipore).

References

1. Cravatt BF, Giang DK, Mayfield SP, Boger DL, Lerner RA and Gilula NB. Molecular characterization of an enzyme that degrades neuromodulatory fatty-acid amides. *Nature*. 1996; 384: 83-7.

2. Devane WA, Hanus L, Breuer A, Pertwee RG, Stevenson LA, Griffin G, Gibson D, Mandelbaum A, Etinger A and Mechoulam R. Isolation and structure of a brain constituent that binds to the cannabinoid receptor. *Science*. 1992; 258: 1946-9.

3. Devane WA, Dysarz FA, 3rd, Johnson MR, Melvin LS and Howlett AC. Determination and characterization of a cannabinoid receptor in rat brain. *Molecular pharmacology*. 1988; 34: 605-13.

4. Munro S, Thomas KL and Abu-Shaar M. Molecular characterization of a peripheral receptor for cannabinoids. *Nature*. 1993; 365: 61-5.

5. Mechoulam R, Ben-Shabat S, Hanus L, Ligumsky M, Kaminski NE, Schatz AR, Gopher A, Almog S, Martin BR, Compton DR and et al. Identification of an endogenous 2-monoglyceride, present in canine gut, that binds to cannabinoid receptors. *Biochem Pharmacol*. 1995; 50: 83-90.

6. Blankman JL, Simon GM and Cravatt BF. A comprehensive profile of brain enzymes that hydrolyze the endocannabinoid 2-arachidonoylglycerol. *Chemistry & biology*. 2007; 14: 1347-56.

7. Herkenham M, Lynn AB, Johnson MR, Melvin LS, de Costa BR and Rice KC. Characterization and localization of cannabinoid receptors in rat brain: a quantitative in vitro autoradiographic study. *The Journal of neuroscience : the official journal of the Society for Neuroscience*. 1991; 11: 563-83.

8. Klein TW, Newton C and Friedman H. Cannabinoid receptors and immunity. *Immunol Today*. 1998; 19: 373-81.

9. Fernandez-Ruiz J, Romero J, Velasco G, Tolon RM, Ramos JA and Guzman M. Cannabinoid CB2 receptor: a new target for controlling neural cell survival? *Trends Pharmacol Sci*. 2007; 28: 39-45.

10. Ranieri R, Laezza C, Bifulco M, Marasco D and Malfitano AM. Endocannabinoid System in Neurological Disorders. *Recent Pat CNS Drug Discov*. 2016; 10: 90-112.

11. Basavarajappa BS, Shivakumar M, Joshi V and Subbanna S. Endocannabinoid system in neurodegenerative disorders. *J Neurochem*. 2017; 142: 624-48.

12. O'Sullivan SE. Endocannabinoids and the Cardiovascular System in Health and Disease. *Handb Exp Pharmacol*. 2015; 231: 393-422.

13. Baker D and Pryce G. The endocannabinoid system and multiple sclerosis. *Curr Pharm Des*. 2008; 14: 2326-36.

14. Karanian DA, Brown QB, Makriyannis A, Kosten TA and Bahr BA. Dual modulation of endocannabinoid transport and fatty acid amide hydrolase protects against excitotoxicity. *The Journal of neuroscience : the official journal of the Society for Neuroscience*. 2005; 25: 7813-20.

15. Baker D, Pryce G, Croxford JL, Brown P, Pertwee RG, Huffman JW and Layward L. Cannabinoids control spasticity and tremor in a multiple sclerosis model. *Nature*. 2000; 404: 84-7.

16. Ohno-Shosaku T, Tsubokawa H, Mizushima I, Yoneda N, Zimmer A and Kano M. Presynaptic cannabinoid sensitivity is a major determinant of depolarization-induced retrograde suppression at hippocampal synapses. *The Journal of neuroscience : the official journal of the Society for Neuroscience*. 2002; 22: 3864-72.

17. Marsicano G, Goodenough S, Monory K, Hermann H, Eder M, Cannich A, Azad SC, Cascio MG, Gutierrez SO, van der Stelt M, Lopez-Rodriguez ML, Casanova E, Schutz G, Zieglgansberger W, Di Marzo V, Behl C and Lutz B. CB1 cannabinoid receptors and on-demand defense against excitotoxicity. *Science*. 2003; 302: 84-8.

18. Monory K, Massa F, Egertova M, Eder M, Blaudzun H, Westenbroek R, Kelsch W, Jacob W, Marsch R, Ekker M, Long J, Rubenstein JL, Goebbels S, Nave KA, During M, Klugmann M, Wolfel B, Dodt HU, Zieglgansberger W, Wotjak CT, Mackie K, Elphick MR, Marsicano G and Lutz B. The endocannabinoid system controls key epileptogenic circuits in the hippocampus. *Neuron*. 2006; 51: 455-66.

19. van der Stelt M, Veldhuis WB, Maccarrone M, Bar PR, Nicolay K, Veldink GA, Di Marzo V and Vliegenthart JF. Acute neuronal injury, excitotoxicity, and the endocannabinoid system. *Mol Neurobiol*. 2002; 26: 317-46.

20. Veldhuis WB, van der Stelt M, Wadman MW, van Zadelhoff G, Maccarrone M, Fezza F, Veldink GA, Vliegenthart JF, Bar PR, Nicolay K and Di Marzo V. Neuroprotection by the endogenous cannabinoid anandamide and arvanil against in vivo excitotoxicity in the rat: role of vanilloid receptors and lipoxygenases. *The Journal of neuroscience : the official journal of the Society for Neuroscience*. 2003; 23: 4127-33.

21. Wallace MJ, Martin BR and DeLorenzo RJ. Evidence for a physiological role of endocannabinoids in the modulation of seizure threshold and severity. *European journal of pharmacology*. 2002; 452: 295-301.

22. Karanian DA, Brown QB, Makriyannis A and Bahr BA. Blocking cannabinoid activation of FAK and ERK1/2 compromises synaptic integrity in hippocampus. *European journal of pharmacology*. 2005; 508: 47-56.

23. Di Marzo V, Melck D, Bisogno T and De Petrocellis L. Endocannabinoids: endogenous cannabinoid receptor ligands with neuromodulatory action. *Trends Neurosci*. 1998; 21: 521-8.

24. Khaspekov LG, Brenz Verca MS, Frumkina LE, Hermann H, Marsicano G and Lutz B. Involvement of brain-derived neurotrophic factor in cannabinoid receptor-dependent protection against excitotoxicity. *Eur J Neurosci*. 2004; 19: 1691-8.

25. Cadas H, Gaillet S, Beltramo M, Venance L and Piomelli D. Biosynthesis of an endogenous cannabinoid precursor in neurons and its control by calcium and cAMP. *The*

Journal of neuroscience : the official journal of the Society for Neuroscience. 1996; 16: 3934-42.

26. Stella N, Schweitzer P and Piomelli D. A second endogenous cannabinoid that modulates long-term potentiation. *Nature*. 1997; 388: 773-8.

27. Kinton L and Duncan JS. Frequency, causes, and consequences of burns in patients with epilepsy. *J Neurol Neurosurg Psychiatry*. 1998; 65: 404-5.

28. Raza M, Pal S, Rafiq A and DeLorenzo RJ. Long-term alteration of calcium homeostatic mechanisms in the pilocarpine model of temporal lobe epilepsy. *Brain Res*. 2001; 903: 1-12.

29. Coomber B, O'Donoghue MF and Mason R. Inhibition of endocannabinoid metabolism attenuates enhanced hippocampal neuronal activity induced by kainic acid. *Synapse*. 2008; 62: 746-55.

30. Ahn K, Johnson DS and Cravatt BF. Fatty acid amide hydrolase as a potential therapeutic target for the treatment of pain and CNS disorders. *Expert opinion on drug discovery*. 2009; 4: 763-84.

31. Lodola A, Castelli R, Mor M and Rivara S. Fatty acid amide hydrolase inhibitors: a patent review (2009-2014). *Expert Opin Ther Pat*. 2015; 25: 1247-66.

32. Bisogno T and Maccarrone M. Latest advances in the discovery of fatty acid amide hydrolase inhibitors. *Expert Opin Drug Discov*. 2013; 8: 509-22.

33. Boger DL, Miyauchi H, Du W, Hardouin C, Fecik RA, Cheng H, Hwang I, Hedrick MP, Leung D, Acevedo O, Guimaraes CR, Jorgensen WL and Cravatt BF. Discovery of a potent, selective, and efficacious class of reversible alpha-ketoheterocycle inhibitors of fatty acid amide hydrolase effective as analgesics. *Journal of medicinal chemistry*. 2005; 48: 1849-56.

34. Mor M, Rivara S, Lodola A, Plazzi PV, Tarzia G, Duranti A, Tontini A, Piersanti G, Kathuria S and Piomelli D. Cyclohexylcarbamic acid 3'- or 4'-substituted biphenyl-3-yl esters as fatty acid amide hydrolase inhibitors: synthesis, quantitative structure-activity relationships, and molecular modeling studies. *Journal of medicinal chemistry*. 2004; 47: 4998-5008.

35. Abouab-Dellah AB, P.; Hoornaert, C.; Jeunesse, J.; Puech, F. . *Patent WO 2004/099176, 2004; US 2006/0089344, 2006*

36. Johnson DS, Stiff C, Lazerwith SE, Kesten SR, Fay LK, Morris M, Beidler D, Liimatta MB, Smith SE, Dudley DT, Sadagopan N, Bhattachar SN, Kesten SJ, Nomanbhoy TK, Cravatt BF and Ahn K. Discovery of PF-04457845: A Highly Potent, Orally Bioavailable, and Selective Urea FAAH Inhibitor. *ACS Med Chem Lett*. 2011; 2: 91-6.

37. Wang X, Sarris K, Kage K, Zhang D, Brown SP, Kolasa T, Surowy C, El Kouhen OF, Muchmore SW, Brioni JD and Stewart AO. Synthesis and evaluation of benzothiazole-based analogues as novel, potent, and selective fatty acid amide hydrolase inhibitors. *Journal of medicinal chemistry*. 2009; 52: 170-80.

38. Gustin DJ, Ma Z, Min X, Li Y, Hedberg C, Guimaraes C, Porter AC, Lindstrom M, Lester-Zeiner D, Xu G, Carlson TJ, Xiao S, Meleza C, Connors R, Wang Z and Kayser F. Identification of potent, noncovalent fatty acid amide hydrolase (FAAH) inhibitors. *Bioorganic & medicinal chemistry letters*. 2011; 21: 2492-6.

39. Huggins JP, Smart TS, Langman S, Taylor L and Young T. An efficient randomised, placebo-controlled clinical trial with the irreversible fatty acid amide hydrolase-1 inhibitor

PF-04457845, which modulates endocannabinoids but fails to induce effective analgesia in patients with pain due to osteoarthritis of the knee. *Pain*. 2012; 153: 1837-46.

40. Chebrou H, Bigey F, Arnaud A and Galzy P. Study of the amidase signature group. *Biochimica et biophysica acta*. 1996; 1298: 285-93.

41. Mileni M, Johnson DS, Wang Z, Everdeen DS, Liimatta M, Pabst B, Bhattacharya K, Nugent RA, Kamtekar S, Cravatt BF, Ahn K and Stevens RC. Structure-guided inhibitor design for human FAAH by interspecies active site conversion. *Proceedings of the National Academy of Sciences of the United States of America*. 2008; 105: 12820-4.

42. Min X, Thibault ST, Porter AC, Gustin DJ, Carlson TJ, Xu H, Lindstrom M, Xu G, Uyeda C, Ma Z, Li Y, Kayser F, Walker NP and Wang Z. Discovery and molecular basis of potent noncovalent inhibitors of fatty acid amide hydrolase (FAAH). *Proceedings of the National Academy of Sciences of the United States of America*. 2011; 108: 7379-84.

43. Tonge PJ. Drug-Target Kinetics in Drug Discovery. *ACS chemical neuroscience*. 2018; 9: 29-39.

44. Schuetz DA, de Witte WEA, Wong YC, Knasmueller B, Richter L, Kokh DB, Sadiq SK, Bosma R, Nederpelt I, Heitman LH, Segala E, Amaral M, Guo D, Andres D, Georgi V, Stoddart LA, Hill S, Cooke RM, De Graaf C, Leurs R, Frech M, Wade RC, de Lange ECM, AP IJ, Muller-Fahrnow A and Ecker GF. Kinetics for Drug Discovery: an industry-driven effort to target drug residence time. *Drug discovery today*. 2017; 22: 896-911.

45. Kalgutkar AS and Dalvie DK. Drug discovery for a new generation of covalent drugs. *Expert Opin Drug Discov*. 2012; 7: 561-81.

46. Nakayama S, Atsumi R, Takakusa H, Kobayashi Y, Kurihara A, Nagai Y, Nakai D and Okazaki O. A zone classification system for risk assessment of idiosyncratic drug toxicity

using daily dose and covalent binding. *Drug metabolism and disposition: the biological fate of chemicals*. 2009; 37: 1970-7.

47. Mileni M, Kamtekar S, Wood DC, Benson TE, Cravatt BF and Stevens RC. Crystal structure of fatty acid amide hydrolase bound to the carbamate inhibitor URB597: discovery of a deacylating water molecule and insight into enzyme inactivation. *Journal of molecular biology*. 2010; 400: 743-54.

48. Mileni M, Garfunkle J, Ezzili C, Kimball FS, Cravatt BF, Stevens RC and Boger DL. X-ray crystallographic analysis of alpha-ketoheterocycle inhibitors bound to a humanized variant of fatty acid amide hydrolase. *Journal of medicinal chemistry*. 2010; 53: 230-40.

49. Meyers MJ, Long SA, Pelc MJ, Wang JL, Bowen SJ, Walker MC, Schweitzer BA, Madsen HM, Tenbrink RE, McDonald J, Smith SE, Foltin S, Beidler D and Thorarensen A. Discovery of novel spirocyclic inhibitors of fatty acid amide hydrolase (FAAH). Part 1: identification of 7-azaspiro[3.5]nonane and 1-oxa-8-azaspiro[4.5]decane as lead scaffolds. *Bioorganic & medicinal chemistry letters*. 2011; 21: 6538-44.

50. Meyers MJ, Long SA, Pelc MJ, Wang JL, Bowen SJ, Schweitzer BA, Wilcox MV, McDonald J, Smith SE, Foltin S, Rumsey J, Yang YS, Walker MC, Kamtekar S, Beidler D and Thorarensen A. Discovery of novel spirocyclic inhibitors of fatty acid amide hydrolase (FAAH). Part 2. Discovery of 7-azaspiro[3.5]nonane urea PF-04862853, an orally efficacious inhibitor of fatty acid amide hydrolase (FAAH) for pain. *Bioorganic & medicinal chemistry letters*. 2011; 21: 6545-53.

51. Ahn K, Johnson DS, Mileni M, Beidler D, Long JZ, McKinney MK, Weerapana E, Sadagopan N, Liimatta M, Smith SE, Lazerwith S, Stiff C, Kamtekar S, Bhattacharya K, Zhang Y, Swaney S, Van Becelaere K, Stevens RC and Cravatt BF. Discovery and characterization of

a highly selective FAAH inhibitor that reduces inflammatory pain. *Chemistry & biology*. 2009; 16: 411-20.

52. Palermo G, Rothlisberger U, Cavalli A and De Vivo M. Computational insights into function and inhibition of fatty acid amide hydrolase. *European journal of medicinal chemistry*. 2015; 91: 15-26.

53. Bracey MH, Hanson MA, Masuda KR, Stevens RC and Cravatt BF. Structural adaptations in a membrane enzyme that terminates endocannabinoid signaling. *Science*. 2002; 298: 1793-6.

54. Ruiz-Castillo P and Buchwald SL. Applications of Palladium-Catalyzed C-N Cross-Coupling Reactions. *Chemical reviews*. 2016; 116: 12564-649.

55. Alapafuja SO, Nikas SP, Bharathan IT, Shukla VG, Nasr ML, Bowman AL, Zvonok N, Li J, Shi X, Engen JR and Makriyannis A. Sulfonyl fluoride inhibitors of fatty acid amide hydrolase. *Journal of medicinal chemistry*. 2012; 55: 10074-89.

56. Patricelli MP, Lashuel HA, Giang DK, Kelly JW and Cravatt BF. Comparative characterization of a wild type and transmembrane domain-deleted fatty acid amide hydrolase: identification of the transmembrane domain as a site for oligomerization. *Biochemistry*. 1998; 37: 15177-87.

57. Ramarao MK, Murphy EA, Shen MW, Wang Y, Bushell KN, Huang N, Pan N, Williams C and Clark JD. A fluorescence-based assay for fatty acid amide hydrolase compatible with high-throughput screening. *Analytical biochemistry*. 2005; 343: 143-51.

58. Zvonok N, Pandarinathan L, Williams J, Johnston M, Karageorgos I, Janero DR, Krishnan SC and Makriyannis A. Covalent inhibitors of human monoacylglycerol lipase:

ligand-assisted characterization of the catalytic site by mass spectrometry and mutational analysis. *Chemistry & biology*. 2008; 15: 854-62.

59. Shields CM, Zvonok N, Zvonok A and Makriyannis A. Biochemical and Proteomic Characterization of Recombinant Human alpha/beta Hydrolase Domain 6. *Scientific reports*. 2019; 9: 890.

60. Abadji V, Lucas-Lenard JM, Chin C and Kendall DA. Involvement of the carboxyl terminus of the third intracellular loop of the cannabinoid CB1 receptor in constitutive activation of Gs. *J Neurochem*. 1999; 72: 2032-8.

61. Dodd PR, Hardy JA, Oakley AE, Edwardson JA, Perry EK and Delaunoy JP. A rapid method for preparing synaptosomes: comparison, with alternative procedures. *Brain Res*. 1981; 226: 107-18.

62. Guo Y, Abadji V, Morse KL, Fournier DJ, Li X and Makriyannis A. (-)-11-Hydroxy-7'-isothiocyanato-1',1'-dimethylheptyl-delta 8-THC: a novel, high-affinity irreversible probe for the cannabinoid receptor in the brain. *J Med Chem*. 1994; 37: 3867-70.

63. Morse KL, Fournier DJ, Li X, Grzybowska J and Makriyannis A. A novel electrophilic high affinity irreversible probe for the cannabinoid receptor. *Life Sci*. 1995; 56: 1957-62.

64. Lan R, Liu Q, Fan P, Lin S, Fernando SR, McCallion D, Pertwee R and Makriyannis A. Structure-activity relationships of pyrazole derivatives as cannabinoid receptor antagonists. *J Med Chem*. 1999; 42: 769-76.

65. Cravatt BF, Wright AT and Kozarich JW. Activity-based protein profiling: from enzyme chemistry to proteomic chemistry. *Annu Rev Biochem*. 2008; 77: 383-414.

66. Clapper JR, Henry CL, Niphakis MJ, Knize AM, Coppola AR, Simon GM, Ngo N, Herbst RA, Herbst DM, Reed AW, Cisar JS, Weber OD, Viader A, Alexander JP, Cunningham ML, Jones

TK, Fraser IP, Grice CA, Ezekowitz RAB, O'Neill GP and Blankman JL. Monoacylglycerol Lipase Inhibition in Human and Rodent Systems Supports Clinical Evaluation of Endocannabinoid Modulators. *The Journal of pharmacology and experimental therapeutics*. 2018; 367: 494-508.

67. DeKosky ST, Scheff SW and Styren SD. Structural correlates of cognition in dementia: quantification and assessment of synapse change. *Neurodegeneration : a journal for neurodegenerative disorders, neuroprotection, and neuroregeneration*. 1996; 5: 417-21.

68. Karanian DA and Bahr BA. Cannabinoid drugs and enhancement of endocannabinoid responses: strategies for a wide array of disease states. *Current molecular medicine*. 2006; 6: 677-84.

69. Naidoo V, Nikas SP, Karanian DA, Hwang J, Zhao J, Wood JT, Alapafuja SO, Vadivel SK, Butler D, Makriyannis A and Bahr BA. A new generation fatty acid amide hydrolase inhibitor protects against kainate-induced excitotoxicity. *Journal of molecular neuroscience : MN*. 2011; 43: 493-502.

70. Farizatto KLG, Ikonne US, Almeida MF, Ferrari MFR and Bahr BA. Abeta42-mediated proteasome inhibition and associated tau pathology in hippocampus are governed by a lysosomal response involving cathepsin B: Evidence for protective crosstalk between protein clearance pathways. *PloS one*. 2017; 12: e0182895.

71. Karanian DA, Karim SL, Wood JT, Williams JS, Lin S, Makriyannis A and Bahr BA. Endocannabinoid enhancement protects against kainic acid-induced seizures and associated brain damage. *The Journal of pharmacology and experimental therapeutics*. 2007; 322: 1059-66.

72. Raveh L, Weissman BA, Cohen G, Alkalay D, Rabinovitz I, Sonego H and Brandeis R. Caramiphen and scopolamine prevent soman-induced brain damage and cognitive dysfunction. *Neurotoxicology*. 2002; 23: 7-17.

73. Zhu X, Liu J, Huang S, Zhu W, Wang Y, Chen O and Xue J. Neuroprotective effects of isoliquiritigenin against cognitive impairment via suppression of synaptic dysfunction, neuronal injury, and neuroinflammation in rats with kainic acid-induced seizures. *International immunopharmacology*. 2019; 72: 358-66.

74. O'Leary H, Bernard PB, Castano AM and Benke TA. Enhanced long term potentiation and decreased AMPA receptor desensitization in the acute period following a single kainate induced early life seizure. *Neurobiology of disease*. 2016; 87: 134-44.

75. Butler D, Bendiske J, Michaelis ML, Karanian DA and Bahr BA. Microtubule-stabilizing agent prevents protein accumulation-induced loss of synaptic markers. *European journal of pharmacology*. 2007; 562: 20-7.

76. Farizatto KLG, Almeida MF, Long RT and Bahr BA. Early Synaptic Alterations and Selective Adhesion Signaling in Hippocampal Dendritic Zones Following Organophosphate Exposure. *Scientific reports*. 2019; 9: 6532.

Figure 1. Known FAAH inhibitors
Figure 2. Explore regional hydrophilic patterns of ligand substitution to improve druggability
Figure 3. Induced-fit docking of 9 with humanized FAAH crystal structure. A Connolly surface shown as electrostatic potential (red-white-blue) was used to represent the shape of the binding pocket. Catalytic residue Ser241 and Phe432, a key residue of the MAC channel, are shown in green. Key residues forming the binding pocket shown in wireframe. The ligand is shown in gray. Atoms are colored by atom type. Hydrogen bonds are indicated by yellow dashed lines, and the distance of catalytic Ser241 from the carbamate group in magenta dashed line.
Figure 4. Covalent docking of **9** with humanized FAAH crystal structure with the leaving group no longer attached. A Connolly surface shown as electrostatic potential (red-white-blue) was used to represent the shape of the binding pocket. Catalytic residue Ser241 and Phe432, a key residue of the MAC channel, are shown in green. Key residues forming the binding pocket shown in wireframe. The ligand is shown in gray. Atoms are colored by atom type. Hydrogen bonds are indicated by yellow dashed lines.
Figure 5. Overlapped covalent docking poses of **9** (green) and **PF-3845** (magenta) with humanized FAAH crystal structure. A Connolly surface shown as electrostatic potential (red-white-blue) was used to represent the shape of the binding pocket. Phe432, a key residue of the MAC channel, is shown in green. Key residues forming the binding pocket are shown in thin tube representation (gray). Atoms are colored by atom type. Hydrogen bonds are indicated by yellow dashed lines, and π-stacking interactions shown in blue dashed lines.
Figure 6. Gel-based ABPP analysis was performed using membrane homogenates prepared from rat brain tissue and the rhodamine-tagged fluorophosphonate (FP-Rh) probe. FAAH inhibitors **9** and **31** completely inhibited FAAH at 1 and 10 μM without significant inhibition of other serine hydrolases. Representative additional brain serine hydrolases are designated based on previous ABPP studies[6].
Figure 7. Synaptic protection mediated by FAAH inhibitors in the hippocampal slice model of kainic acid (KA)-induced excitotoxicity. Hippocampal tissue from 12-day-old rats was removed and transverse slices of 400-μm thickness prepared (A), the slices being maintained in six-well culture plates and exhibiting intact neuronal subfields (B). Stable neuronal density determined by Nissl as well as pre- and postsynaptic marker staining was consistently found after several weeks in culture (C, width of view-fields: 1.5 mm). The experimental design includes control slices treated with vehicle only, as well as a 1-h pre-treatment step with vehicle (veh, 0.01% DMSO), FAAH inhibitor compound **9** (AM11994), or compound 31 (AM11987) before a 2-h KA insult with continued presence of vehicle or inhibitor (D). After washout of KA, the cultured slices were incubated with vehicle or FAAH inhibitor for 24 h, followed by harvesting of the brain tissue for subsequent analyses. In order to evaluate potential synaptic protection by compounds 31 (E) and 9 (F), equal protein aliquots of homogenized samples from the different treatment groups were assessed by immunoblot for GluR1, synapsin IIa and IIb (syn IIa and IIb), synaptophysin (SNP), and actin. Integrated optical density measures for GluR1 are shown as means ± SEM (G). Unpaired t-tests compared to KA insult alone: **$p<0.01$ (two-tailed), *$p=0.0292$ (one-tailed).

Figure 8. Pre- and postsynaptic protection by FAAH inhibitor AM11994 (compound 9) in the excitotoxic hippocampal slice. Mature slice cultures were treated with vehicle only, or pre-treated with vehicle or FAAH inhibitor compound **9** (AM11994) for 1 h before the 2-h KA insult step. After washout of KA, slices were incubated with vehicle or compound **9** for the 24-h post-

insult period, then fixed and double immunostained with anti-GluR1 (red) and anti-synaptophysin (green). Size bars: 100 μm. DG, dentate gyrus; sp, stratum pyramidale; sr, stratum radiatum.

Scheme 1

Reagents and conditions: (a) Divinyl sulfone, boric acid, glycerol (cat.), water, reflux, 3 h; (b) benzyl bromide, K_2CO_3, DMF; (c) thiomorpholine 1,1-dioxide or1-methylpiperazine, $Pd_2(dba)_3$, BINAP, NaOtBu, toluene 110 ^oC; (d) H_2, Pd/C, EtOH; (b); (e) 3 bis(pentafluorophenyl) carbonate, N,N-diisopropylethylamine, 0 ^oC to rt, 2h; (f) 4, N,N-diisopropylethylamine, 0 ^oC to rt, 2h.

Scheme 2

Reagents and conditions: (a) $Pd_2(dba)_3$, 2-(di-tert-butylphosphino)biphenyl, sodium *tert*-butoxide, pyrrolidine, toluene, 80 ^oC, 12h; (b)1-bromo-2-fluoroethane, K_2CO_3, CH_3CN, 80 ^oC, 16h; (c) TFA, CH_2Cl_2 6h, rt; (d) 3-(1,1-dioxidothiomorpholino)phenyl (perfluorophenyl) carbonate, N,N-diisopropylethylamine, 0 ^oC to rt, 2h.

Scheme 3

Reagents and conditions: (a) i. $Pd_2(dba)_3$, 2-(di-tert-butylphosphino) biphenyl, sodium tert-butoxide, *tert*-butyl (R)-2-methylpiperazine-1-carboxylate, 80 ^oC, 12h; ii. (R)-2-methylpiperazine toluene, 2,2'-bis(diphenylphosphino)-1,1'-binaphthyl and (S)-2-methylpiperazine, 80 ^oC, 12h; (b) TFA, CH_2Cl_2, 6h, rt; (c) 3 (scheme 1), N,N-diisopropylethylamine, 0 ^oC to rt, 2h

Figure 1

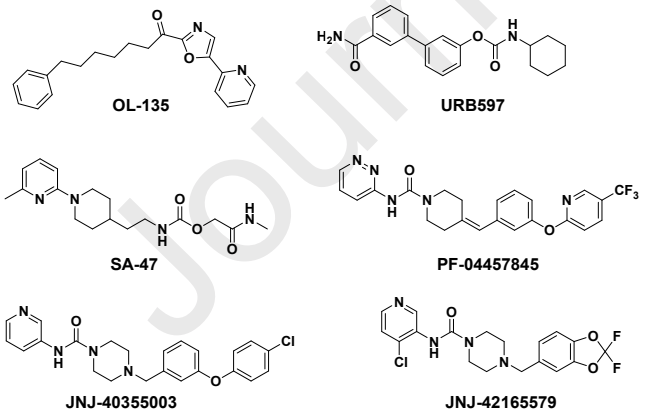

Figure 2

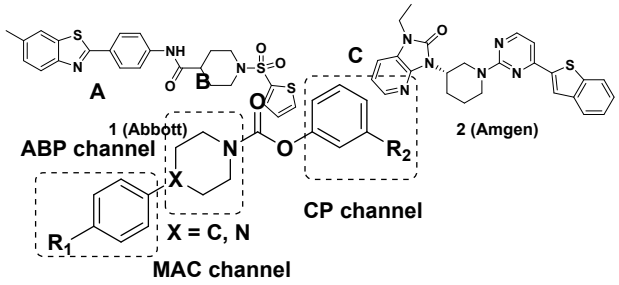

Figure 3

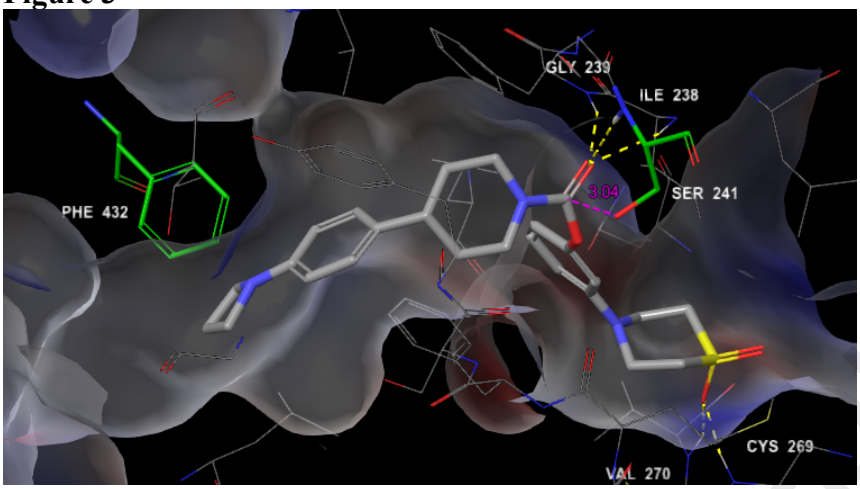

Figure 4

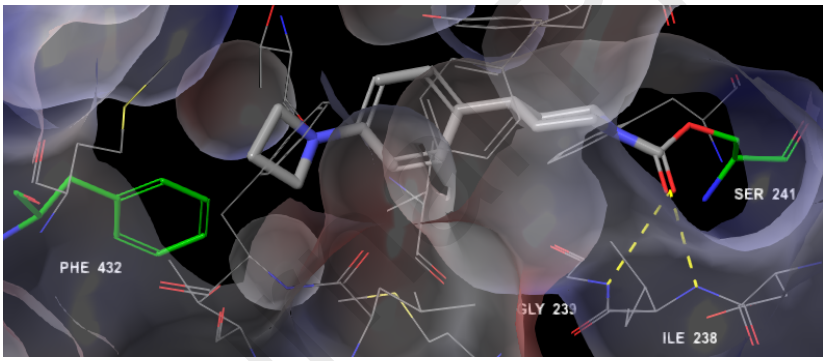

Figure 5

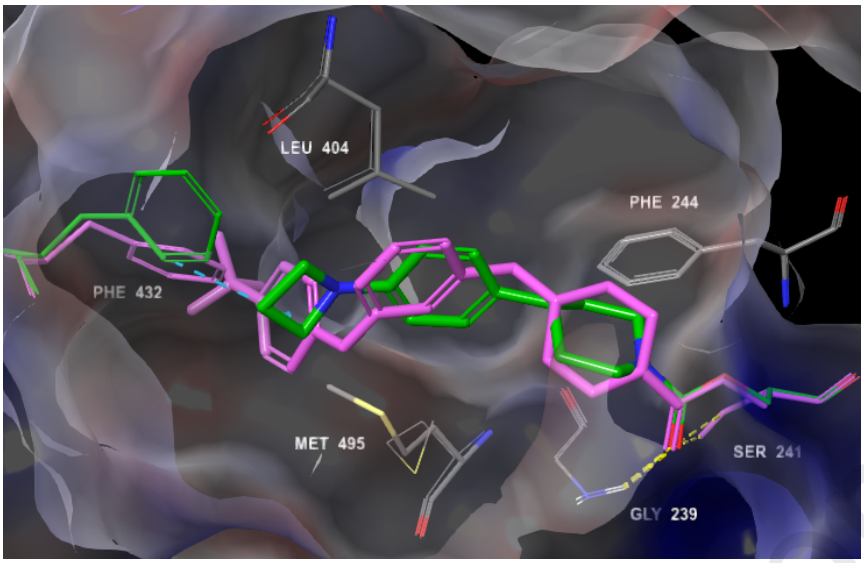

Figure 6

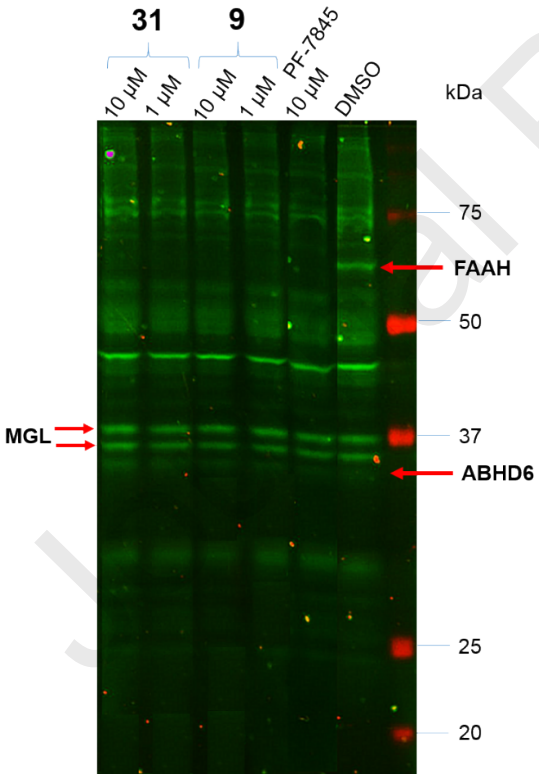

Figure 7

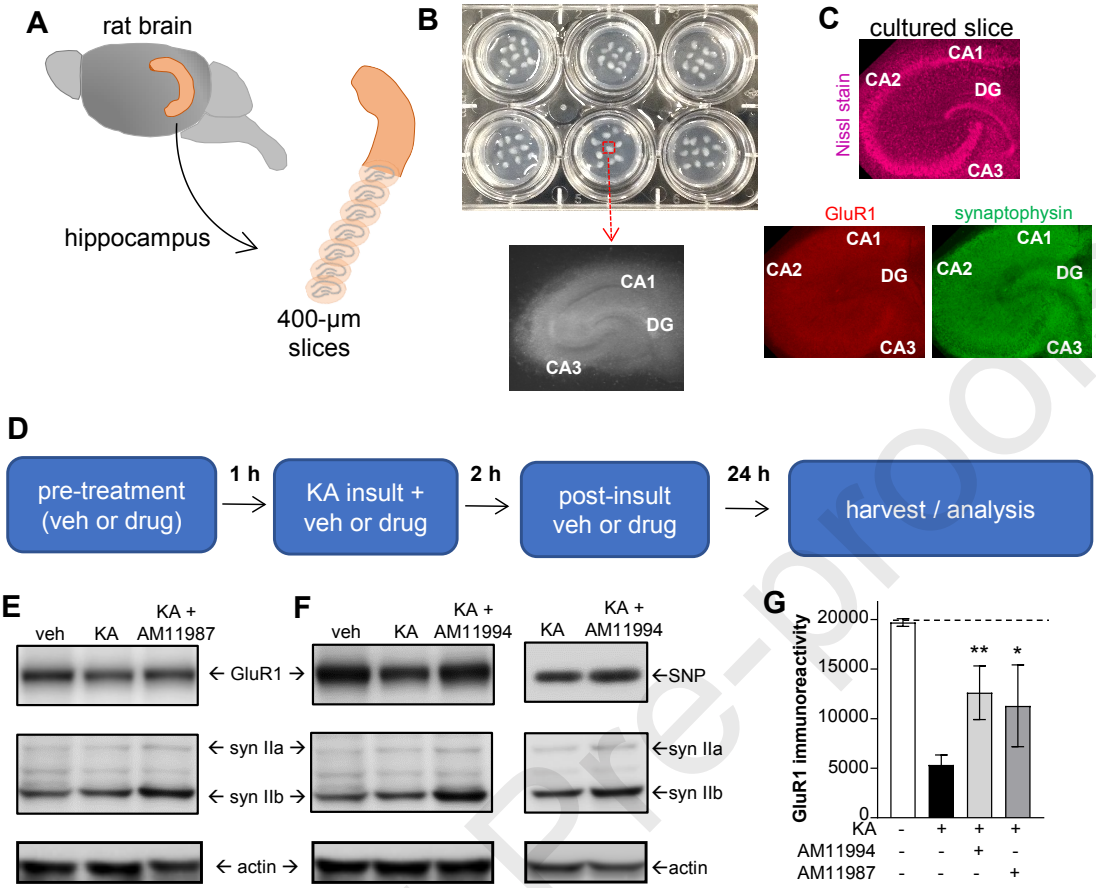

Figure 8

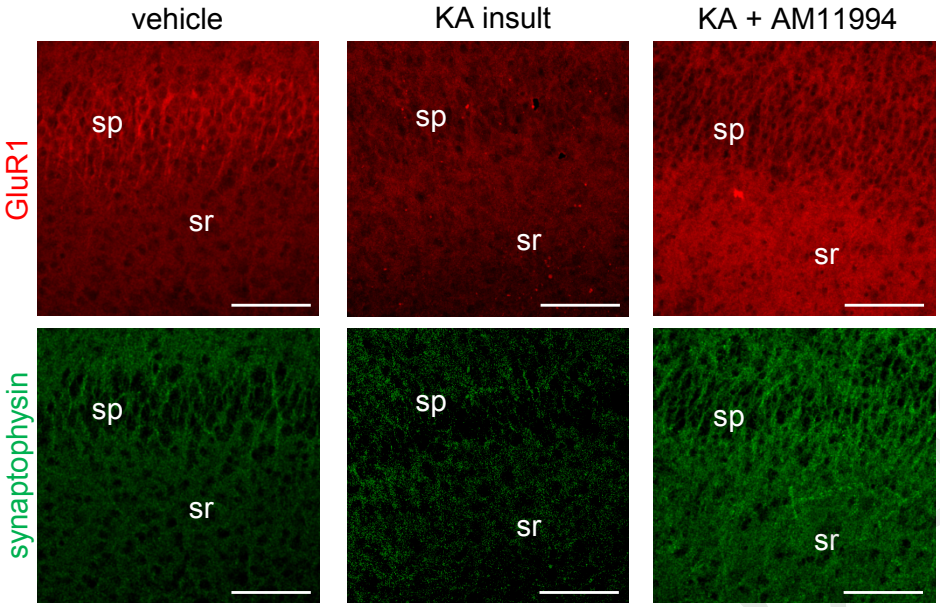

Scheme 1

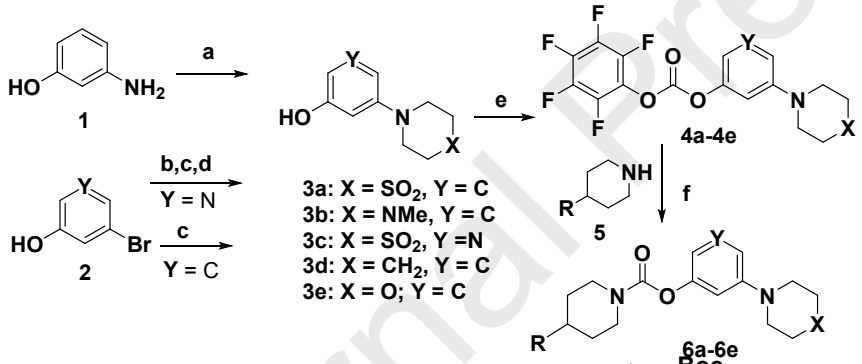

Scheme 2

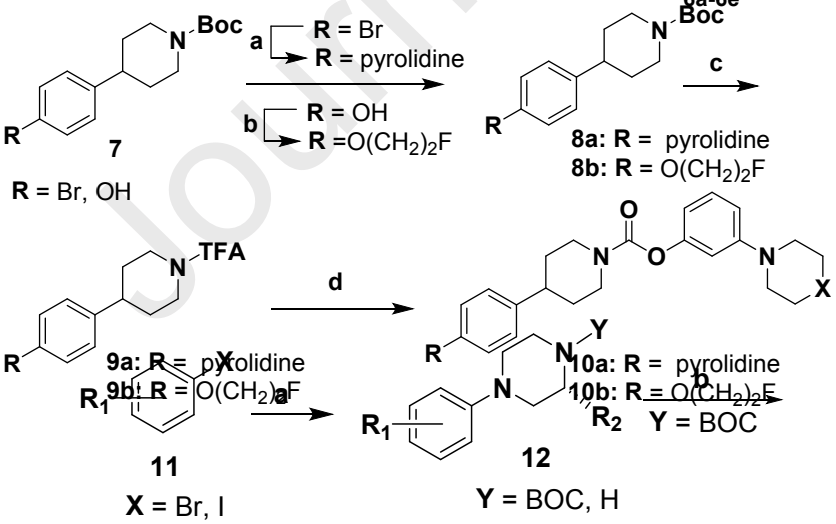

Scheme 3

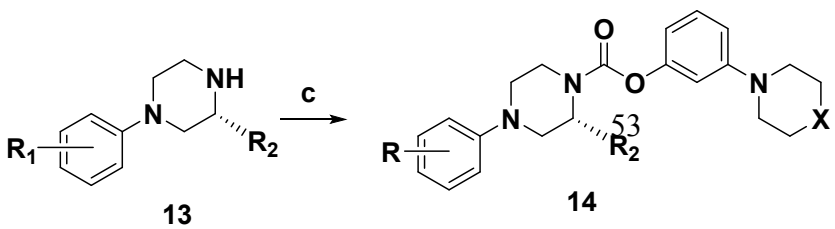

Table 1. Piperidine-carbamates FAAH inhibitors as neuroprotective drugs

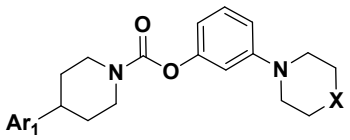

			IC_{50} nM[a]			
Compd	**Ar_1**	**X**	**rFAAH**	**hFAAH**	**hMGL**	**ClogP[c]**
1	Ph	SO2	6.0±01[b]	8.0±0.2	>1000	2.62
2	4-FPh,	SO_2	2.3±0.2	10.0±0.7	>1000	2.76
3	4-OMePh	SO_2	2.61±0.05	6.3±1.4	>1000	2.54
4	4-OCF_3Ph	SO_2	4.0±0.1	3.7±0.3	>1000	3.65
5	4-CNPh	SO_2	9.9±0.1	22.7±1.9	>1000	2.05
6	4-OCH_2CH_2F-Ph	SO_2	5.5+0.2	21.2±0.9	>1000	2.79
7	2-MePh	SO_2	10.3±1.1	15.9±1.1	>1000	3.07
8	4-N,N-dimethyl Ph	SO_2	6.9±0.3	2.4±0.4	>1000	2.78
9	4-azetidyl-Ph	SO_2	5.8±0.2	7.9±1.0	>1000	2.34
10	4-pyrrolidyl-Ph	SO_2	6.3±0.3	3.5±2.2	>1000	2.90
11	4-pyridyl	SO_2	75.5±8.1	131.6±11.1	>1000	1.12
12	3-methyl-1,2,4-oxadiazolyl	SO_2	120±6.5	147.4±11.4	>1000	0.01
13	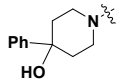	SO_2	78.1±14.3	172.2±10.3	>1000	0.98
14	oxetaneyl	SO_2	NA[d]	NA	>1000	-0.3
15	4-FPh	O	2.93±0.06	16.3±1.3	>1000	3.73

16	4-N,N-dimethyl-Ph	O	14.7±1.1	31.0±7.2	>1000	3.75
17	4-FPh	CH	6.8±0.2	40±4.2	>1000	5.10
18	4-FPh	N-CH_3	9.4±0.5	33.2±2.1	>1000	4.23
19	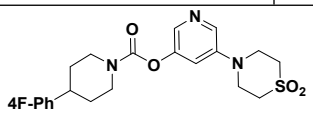		7.1±0.5	4.9±0.7	>1000	2.21
20	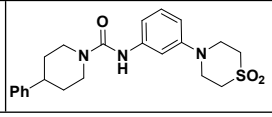		NA	NA	NA	1.75

[a] Inhibition data for h/rFAAH and hMGL were determined using throughput fluorescent assays. [b]IC_{50} ± SD values were determined from triplicate experiments. IC_{50} values were calculated using Prism software (GraphPad). [c] ClogP values were calculated using ChemDraw, version 18.2; [d]NA=not active at 1 uM.

Table 2. Piperazine carbamates FAAH inhibitors as neuroprotective drugs

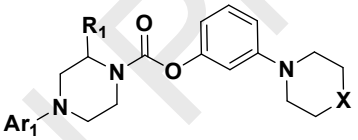

				IC_{50} nM[a]			
Compd	**Ar_1**	**R_1**	**X**	**rFAAH**	**hFAAH**	**hMGL**	**ClogP[c]**
21	Ph	H	SO_2	8.0±0.1[b]	15.0±0.5	>1000	1.93
22	4-F Ph	H	SO_2	12.5±0.3	20.5±2.1	>1000	2.24
23	4-CN Ph	H	SO_2	62.7±3.5	89.3±8.3	>1000	1.76
24	2-pyridyl	H	SO_2	102.3±6.5	ND[d]	>1000	0.98
25	4-pyridazinyl	H	SO_2	NA[e]	NA	>1000	0.03
26	3-Ph-benzyl	H	SO_2	2.1±0.1	1.9±0.1	>1000	4.11
27	3-PhO-benzyl	H	SO_2	2.2±0.5	2.3±0.3	>1000	4.32
28	Ph	(RS)-Me	SO_2	5.5±0.5	2.6±0.1	>1000	2.45
29	Ph	(R)-Me	SO_2	5.7±0.2	17.7 ±3.4	>1000	2.45

30	Ph	(S)-Me	SO_2	NA	NA	ND	2.45
31	4-F Ph	(R)-Me	SO_2	6.3±0.5	11.7±2.6	>1000	2.76
32	4-F Ph	(S)-Me	SO_2	40.5±1.4	72.9±4.5	>1000	2.76
33	4-OMe	(R)-Me	SO_2	7.4±0.3	11.1±1.0	>1000	2.47
34	4-OMe	(R)-Me	O	5.2±0.9	4.1±1.8	>1000	3.43
35	4-OMe	(S)-$CHMe_2$	SO_2	NA	NA	ND	3.69
36	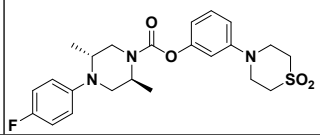			35% @ 1uM	ND	ND	3.28
37	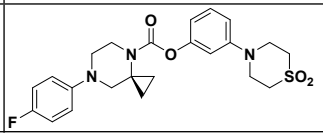			54% @ 1uM	ND	ND	2.56
38	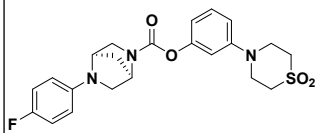			17.1±0.9	20.3±2.4	>1000	2.0
39	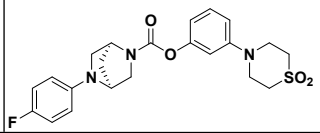			341±12	67% @ 1uM	>1000	2.0
40	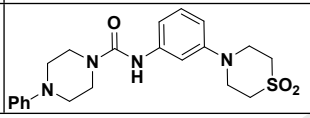			NA	NA	NA	1.29

[a] Inhibition data for h/rFAAH and hMGL were determined using throughput fluorescent assays. [b]IC_{50} ± SD values were determined from triplicate experiments. IC_{50} values were calculated using Prism software (GraphPad). [c] ClogP values were calculated using ChemDraw, version 18.2; [d]ND = not determined; [e]NA=not active at 1 uM.

Table 3. Cassette pharmacokinetics experiments of brain permeability

Compd	**2**	**15**	**8**	**6**
15 min IV brain (μg/mL)	1.23 ± 0.18	0.508 ± 0.034	1.11 ± 0.21	0.909 ± 0.158
15 min IV plasma (μg/mL)	0.474 ± 0.066	0.506 ± 0.056	0.746 ± 0.121	0.388 ± 0.062

Cassette pharmacokinetics at 2 mg/kg, iv. The compounds were brain permeable by comparing brain and plasma levels after iv administration at 15 min

We wish to confirm that there are no known conflicts of interest associated with this publication and there has been no significant financial support for this work that could have influenced its outcome.
We confirm that the manuscript has been read and approved by all named authors and that there are no other persons who satisfied the criteria for authorship but are not listed. We further confirm that the order of authors listed in the manuscript has been approved by all of us.
We confirm that we have given due consideration to the protection of intellectual property associated with this work and that there are no impediments to publication, including the timing of publication, with respect to intellectual property. In so doing we confirm that we have followed the regulations of our institutions concerning intellectual property.
We further confirm that any aspect of the work covered in this manuscript that has involved either experimental animals or human patients has been conducted with the ethical approval of all relevant bodies and that such approvals are acknowledged within the manuscript. We understand that the Corresponding Author is the sole contact for the Editorial process (including Editorial Manager and direct communications with the office). He/she is responsible for communicating with the other authors about progress, submissions of revisions and final approval of proofs. We confirm that we have provided a current, correct email address which is accessible by the Corresponding Author and which has been configured to accept email from (m.malamas@northeastern.edu)

Michael Malamas, PhD.

Graphical Abstract

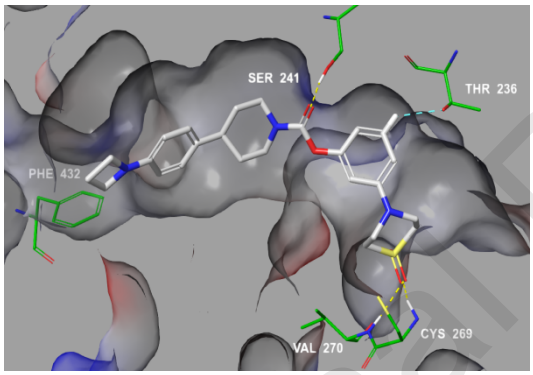

Precovalent docking of FAAH inhibitor **9** at "humanized" rat FAAH's active site.

AMPA receptor subunit GluR1

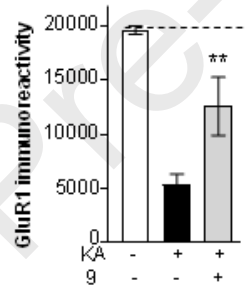

Synaptic protection of **9** in hippocampal slice cultures after kainic acid-induced excitotoxicity.